

UNIVERSITÉ DE GENÈVE
Section de chimie et biochimie
Department de biochimie

FACULTÉ DES SCIENCES
Professeur Marko Kaksonen

Regulation of membrane scission in yeast endocytosis

THÈSE
présentée à la Faculté des sciences de l'Université de Genève
pour obtenir le grade de Docteur ès sciences, mention biochimie

par
Deepikaa Menon
de
Chennai (India)

Thèse N° xxxx

GENÈVE / HEIDELBERG
photoshop EMBL
2018

Abstract

Endocytosis is an ancient pathway that regulates communication of the cell with its environment. During this process, the plasma membrane is deformed in a controlled sequence: a flat membrane forms an invagination that undergoes scission to produce a cargo-filled vesicle. Breaking the membrane invagination to form a vesicle is perhaps the most dramatic shape transition in this development. This has excited a large body of literature on the cause of membrane scission. Work on mammalian cells has converged on a scission mechanism based on membrane neck constriction by the GTPase dynamin. A clear understanding of what causes scission remains incomplete for the much simpler endocytic network in yeast cells.

In this thesis, I investigate the mechanism of membrane scission in *Saccharomyces cerevisiae* and the proteins involved by combining mutagenesis with live-cell imaging of fluorescently tagged proteins.

Endocytic sites are very stereotypic in yeast, recruiting about 50 proteins- most with mammalian homologues- in a highly specific sequence. These proteins can be assigned to separable modules based on their role in the endocytosis. Members of the coat module arrive when the membrane is still flat and form the template for invagination. Actin regulators arrive later and produce the forces required to pull up the membrane. Scission proteins arrive at the end of the timeline and regulate vesicle formation.

The yeast BAR domain complex Rvs is an important regulator of scission: in cells without Rvs, scission efficiency decreases by nearly 30%. The 70% of invaginations that undergo scission in the cells form smaller vesicles than usual. Rvs thus appears to regulate both timing and likelihood of scission, but it has not been clear how it does so, or how it gets recruited to membrane tubes in the first place.

I find that Rvs localization is timed by its BAR domain. The BAR domain senses a particular membrane shape, and Rvs is only recruited to endocytic sites once this shape is acquired. Surprisingly, localization efficiency and localization itself is affected by a second domain of Rvs167, the SH3 domain. This domain helps recruitment of Rvs and likely couples the actin network to vesicle scission, triggering disassembly of the actin network once scission occurs.

Several models have been proposed for what eventually causes scission. I test predictions of some of these models. I find that forces generated by dynamin and lipid hydrolysis do not drive vesicle formation. Scission timing is also independent of the number of BAR domains recruited to membrane tubes, so is not based on BAR concentration-dependent membrane rupture. This timing is instead regulated by the amount of actin at endocytic sites, and hence by the magnitude of forces generated on the membrane. There appears to be a threshold force over which the membrane reliably ruptures. The function of Rvs is to scaffold the membrane, and prevent scission before this force is generated, allowing reliable formation of vesicles.

Zusammenfassung

Clathrin-vermittelte Endozytose ist ein essentieller zellulärer Prozess, um Moleküle von der Zelloberfläche aufzunehmen. Mehr als 50 Proteine bilden die zugrundeliegende makromolekulare Maschinerie, welche in Eukaryoten höchst konserviert ist. Um ihre Konstruktionsweise zu verstehen, welche eine Vesikelbildung mit hoher Effizienz und Regelmäßigkeit erlaubt, ist es notwendig zu untersuchen, wie endozytotische Proteine strukturell organisiert sind. Aufgrund der kleinen Größe, Komplexität und Dynamik der endozytotischen Maschinerie ist die Anordnung dieser Proteine *in situ* jedoch größtenteils unbekannt.

Ich habe Einzelmolekül-Lokalisationsmikroskope verwendet, um endozytotische Strukturen in fixierten Zellen von Bäckerhefe *Saccharomyces cerevisiae* mit hoher räumlicher Auflösung abzubilden. Dabei habe ich eine komplexe Organisation der endozytotischen Proteinen festgestellt.

Mithilfe von Hochdurchsatz-Lokalisationsmikroskopie konnte ich zehntausende endozytotische Strukturen untersuchen. Dabei habe ich eine bemerkenswerte radiale Ordnung gefunden, in welcher die funktionalen Module festgelegte radiale Bereiche besetzen. Je weiter Endozytose fortgeschreitet, desto größer und regelmäßiger werden die Strukturen. Zu Beginn sind die Anordnungen vielfältig in Größe und Form, während sie später einen hohen radialen Organisationsgrad aufweisen. Ich habe entdeckt, dass Aktin-Polymerisation, welche in Hefe zur Endozytose benötigt wird, nur in einem durch Aktin-Nukleirungsfaktoren bestimmten, ringförmigen Bereich auftritt. Dieser Bereich bildet sich um eine Proteinschicht herum, in welcher Proteine die Plasmamembran mit dem Aktinnetzwerk verknüpfen. Durch dieses Ringmuster kann die notwendige Kraft, um die Plasmamembrane einzustülpen, durch die Bildung eines Aktinnetzwerkes effizient erzeugt und auf die Membran übertragen werden. In einem äußeren Ring zieht ein endozytotischer Myosin-Motor möglicherweise das Aktin-Netzwerk auseinander, um den Einstülpungsprozess zu unterstützen.

Ich habe ein neues Konzept entwickelt, um den endozytotischen Zeitpunkt von fixierten Strukturen direkt aus den hochauflösten Bildern zu bestimmen, indem sie mithilfe von Fluoreszenz-Partikelverfolgungs-Daten aus lebenden Zellen ausgewertet werden. Dadurch konnte ich die höchst dynamische mobile Phase der Endozytose mit zeitlicher und hoher räumlicher Auflösung darstellen. Diese Visualisierung zeigte direkt, dass sich das Aktin-Netzwerk aus einer Nukleierungszone auf der Plasmamembran bildet, welche durch Nukleirungsfaktoren gebildet wird.

Ich schlage deshalb ein Modell vor, wie sich die endozytotische Maschinerie organisiert. Nach einer Initiierungsphase mit variablem Zeitablauf und vielfältigen Strukturen gibt es einen Übergang hin zu regelmäßigen, radial organisierten Proteinanordnungen, welche sich um die zentrale Proteinschicht bilden. Durch diese Organisation wird ein Bereich robust vorbestimmt, in welchen sich später das Aktin-Netzwerk bilden kann. Der Beginn der Aktin-Polymerisierung ist ein wichtiger mechanistischer Schritt, der den Übergang hin zur mobilen Phase der Endozytose bewirkt, in welchem schließlich das Clathrin-umhüllte Vesikel gebildet wird.

Acknowledgements

Thank you Marko, for your patience and guidance while I discovered biology, whether or not you realized what you were getting into. I feel (gratuitously) lucky to have been supervised by someone with whom I share a philosophy of science. Many thanks to the lab: Ori, Camilla, Hetty, Tanja, and Andrea, for getting me started on the messy details, your invaluable feedback throughout, and for making coming to work fun. The Geneva crew, Daniel, Mateusz, Serena, and Anne-Sophie, thanks for the many animated discussions, and for sharing weird work hours!

Thanks to Jonas and the rest of the Ries lab for shelter during the transition to Geneva. Jonas, I'm still a bit skeptical about whether it's actually healthy to eat that fast, but I will keep trying. Joran, Markus, Kostek, Jan, thank you for making limbo bearable. Markus, for the many conversations, meals, and for annoying me into becoming a better scientist. I am delighted to be the other grumpy person.

Noticeably complacent about expressing my feelings, I will take the opportunity to thank the people I am deeply indebted to for getting me through these years. Thibaut, Martina and Paul, I have been rescued many times only by your existence, thank you for existing. Anastasia, for sharing your home and friendship. Many others in Heidelberg and Geneva who have made this time enjoyable: Filipa, Marvin, Phillippe, Ori, Daniel, thank you for the company.

Last and quite far from least, the fact that this thesis exists is owed to Helke Hildebrand, Dean of the Graduate program at EMBL when I started my PhD. Thank you Helke, for the endless supply of support, encouragement, and chocolate. ori

First and foremost: Thank you Jonas, for inviting me to join your group when it had just become one, and for sharing this truly exciting time of starting a lab, when ideas turn into projects, and rooms that seem large become too small. I am really grateful for your guidance and support, your openness to my ideas and the freedom to pursue them, for keeping your door open at all times, for your physicist's approach to thinking about biology, and your respectful and enjoyable

way of leading the lab. It was really fruitful and fun working with you over the past four years.

Contents

Abstract	3
Zusammenfassung	5
Contents	9
1 Introduction	1
1.1 Endocytosis and cell trafficking pathways	1
1.2 Clathrin-mediated endocytosis	3
1.3 CME in mammalian and yeast cells	5
1.3.1 Clathrin is required for mammalian CME	5
1.3.2 Actin forces are required for yeast CME	6
1.3.3 CME in yeast is highly regular	6
1.3.3.1 Early initiation phase	7
1.3.3.2 Coat module	8
1.3.3.3 Actin module	8
1.3.3.4 Scission module	9
1.3.4 Membrane scission in mammalian cells	9
1.3.4.1 Scission is dependent on dynamin	9
1.3.4.2 Dynamin is an oligomeric GTPase	10
1.3.4.3 Dynamin interacts with BAR proteins to cause scission	10
1.3.4.4 Dynamin and BAR proteins interact via PRD and SH3 regions	11
1.3.5 Membrane scission in yeast	11
1.3.5.1 Yeast dynamin-like proteins	11
1.3.5.2 Yeast BAR domain proteins Rvs161/167 regulate scission timing	12
1.3.5.3 What causes scission?	12
1.4 BAR domain proteins	14

1.4.1	NBAR proteins and membrane shapes	15
1.4.2	NBAR protein in endocytosis: Amphiphysin . .	16
1.4.3	NBAR protein in endocytosis: Endophilin . . .	16
1.4.4	NBAR protein in yeast endocytosis: the Rvs complex	17
2	Aims of the study	19
3	Results	21
3.1	Tracking endocytic proteins in yeast	21
3.2	Rvs deletion phenotype	24
3.3	Recruitment of Rvs and function of domains	25
3.3.1	BAR domains sense membrane curvature in-vivo	26
3.3.2	The SH3 domain is able to localize Rvs in an actin and curvature-independent manner	28
3.3.3	Loss of the SH3 domain affects progression of endocytic sites	30
3.4	Function of Rvs	32
3.4.1	BAR domains as scaffold for dynamin	32
3.4.1.1	Vps1 does not affect Sla1 or Rvs167 dynamics	35
3.4.2	Yeast synaptojanins do not significantly affect coat and Rvs movement	38
3.4.3	Membrane scission does not occur at shorter tube lengths with more Rvs	43
3.4.4	Coat movement is influenced by recruitment of BAR domain	50
3.4.5	Requirement for Rvs is unchanged by membrane tension	54
4	Discussion	57
4.1	Recruitment of Rvs to endocytic sites	57
4.1.1	The BAR domain senses membrane curvature .	58
4.1.2	BAR domain times recruitment of Rvs	58
4.1.3	The SH3 domain makes Rvs recruitment efficient	59
4.1.4	The SH3 domain can assemble and disassemble Rvs molecules independent of the BAR domain and actin interactions	59
4.1.5	SH3 domain times affects actin dynamics	60

4.1.6	What does the SH3 domain interact with?	60
4.1.7	Total number of Rvs recruited is independent of ploidy	61
4.1.8	Rvs recruitment rate increases with increasing gene copies	62
4.2	Arrangement of Rvs	64
4.2.1	Rvs does not form a tight scaffold on membrane tubes	64
4.2.2	A limit for how much Rvs can be recruited to the membrane	65
4.3	What causes membrane scission?	67
4.3.1	Dynamin does not drive scission	67
4.3.2	Lipid hydrolysis is not the primary cause of membrane scission	67
4.3.3	Protein friction does not drive membrane scission	69
4.3.4	Actin polymerization generates forces required for membrane scission	69
4.4	Function of the Rvs complex	70
4.4.1	Rvs scaffolds membrane pore	70
4.4.2	A critical amount of Rvs is required to stabilize the membrane	71
4.5	Role of other scission-stage proteins	72
4.5.1	Inp52 is likely involved in uncoating vesicles after scission	72
4.6	Model for membrane scission	72
4.7	Other potential scission mechanisms and open questions	73
5	Materials and Methods	75
5.1	Materials	76
5.1.1	Yeast strains	76
5.1.2	Plasmids	80
5.1.3	Buffers	81
5.1.4	Media	81
5.1.5	Imaging	83
5.2	Methods	84
5.2.1	Fluorescent tagging yeast with PCR cassette insertion	84
5.2.2	Live-cell imaging	84
5.2.2.1	Live-cell Image analysis	85

5.2.2.2	Cytoplasmic background quantification for BAR versus WT Rvs167-GFP	86
5.2.2.3	CLEM	87
Bibliography		90

List of Figures

3.1	Tracking yeast endocytic proteins	23
3.2	Coat movement in <i>rvs167Δ</i> cells	24
3.3	Localization of the Rvs167 BAR domain	29
3.4	Tracking endocytic proteins in BAR cells	33
3.5	Phenotype of <i>vps1Δ</i>	35
3.6	Tracking endocytic proteins in <i>vps1Δ</i> cells	36
3.7	Synaptojanin-like proteins in yeast	39
3.8	Effect of synaptojanin deletion	41
3.9	Overexpression of Rvs in haploid cells	45
3.10	Titration of Rvs molecule numbers in diploid cells . . .	48
3.11	Molecule numbers in diploid cells	49
3.12	Overexpression of the Rvs BAR domain	52
3.13	Effect of sorbitol on <i>rvs167Δ</i> cells	55
4.1	Synaptojanin-like proteins in yeast	62
4.2	Synaptojanin-like proteins in yeast	63
4.3	Synaptojanin-like proteins in yeast	66

List of Tables

3.1 Median molecule number of Rvs167 and Abp1	56
---------------------------------------------------------	----

List of Abbreviations

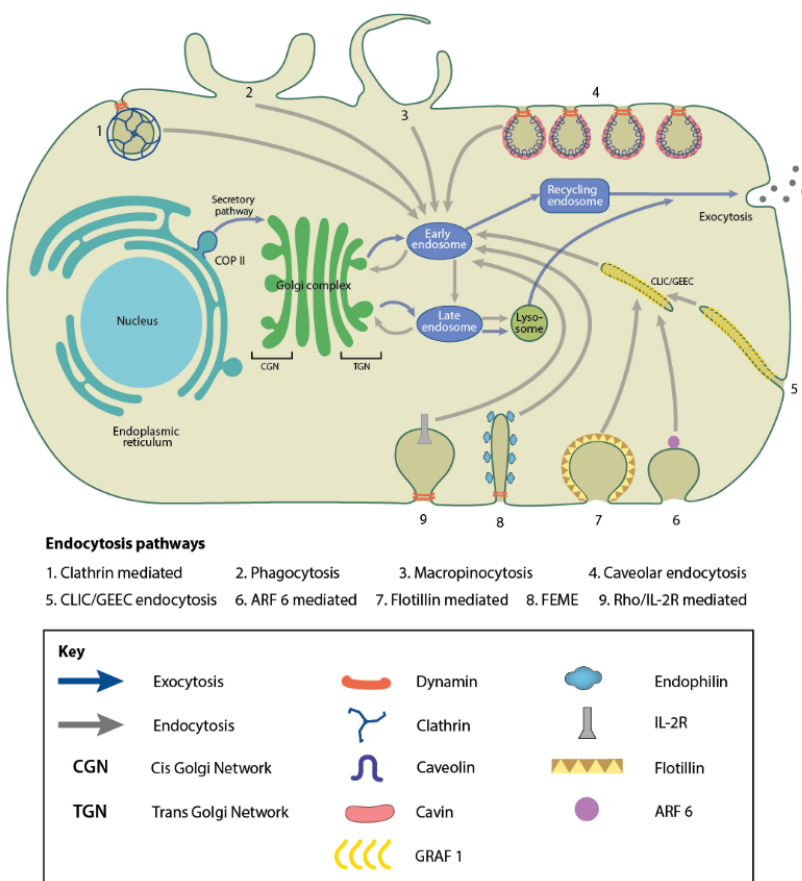
2D	Two-dimensional
3D	Three-dimensional
ATP	Adenosine triphosphate
ANTH	AP180 N-terminal homology
CME	Clathrin-mediated endocytosis
ConA	Concanavalin A
CLEM	Correlative light and electron microscopy
DNA	Deoxyribonucleic acid
EDTA	Ethylene diamine tetraacetate
EE	Early endosome
EM	Electron microscopy
EMCCD	Electron multiplying charge-coupled device
ENTH	Epsin N-terminal homology
ER	Endoplasmic reticulum
FRAP	Fluorescence recovery after photobleaching
MVB	Multivesicular body
NPF	Nucleation promoting factor
ORF	Open reading frame
OD₆₀₀	Optical density (600 nm)
PBS	Phosphate buffered saline
PIP₂	Phosphatidyl inositol (4,5) diphosphate
PEG	Poly ethylene glycol
PM	Plasma membrane
PCR	Polymerase chain reaction
RFP	Red fluorescent protein
ROI	Region of interest
RNA	Ribonucleic acid
RT	Room temperature
SH3	Src homology 3

SC	Synthetic complete
TIRF	Total internal reflection fluorescence
UV	Ultra violet
WH	WASP homology
WASP	Wiskott-Aldrich syndrome protein
WT	Wild-type
YPD	Yeast extract peptone dextrose
YPAD	Yeast extract peptone dextrose plus adenine

1 | Introduction

1.1 Endocytosis and cell trafficking pathways

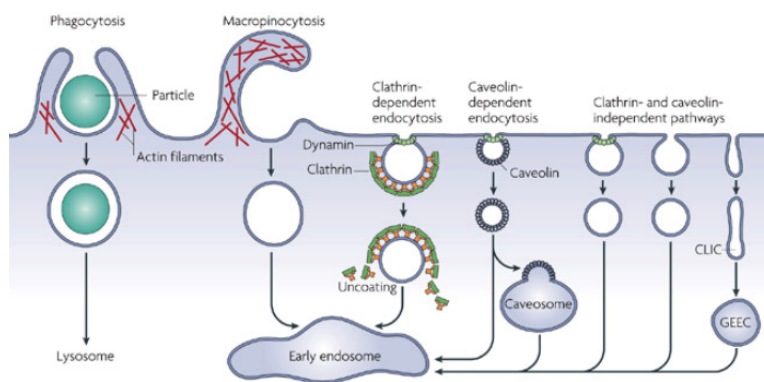
The plasma membrane serves as the defining barrier between the internal and external cell, thus creating cellular identity, and facilitating evolution out of the primordial soup into a defined structure that can regulate entry of signals into the cell. In eukaryotes, and with increasing complexity, in multicellular eukaryotes, tuning cellular response to external signals has resulted in a complex network of signaling pathways, and tight coupling of these pathways with the process of endocytosis. Endocytosis is defined as the uptake of molecules too big to pass through the plasma membrane. It involves the invagination of the plasma membrane into a cargo-filled tube, and culminates in the severing of this tube to form a cargo-filled vesicle, whose components and contents are then targeted to other cellular organelles for either degradation or recycling.



Apart from internalizing cargo, endocytosis allows regulation of the plasma membrane itself: its lipid and protein composition, and therefore many physical and biochemical properties like tension, rigidity, surface-receptor composition and localization. Cargo taken up by endocytic pathways include these surface-receptors and their ligands, that are transported across the cell, taking part in a signaling cascade, and forming the link between cell signaling and endocytosis.

Somewhat dramatically, endocytosis “constitutes the major communications infrastructure of the cell. As such, it governs almost all aspects of the relationships of the cell with the extracellular environment and of intracellular communication. Its evolution constitutes, arguably, the major driving force in the evolution of prokaryotic to eukaryotic organisms”¹. Plasma membrane regulation and internalization of signaling molecules are critical for the function of the cell. Among the vast array of important cargo that are taken up via endocytosis are cholesterol^{2,3}, insulin⁴, and other hormones. Not surprisingly, many human diseases have been linked to defects in the endocytic pathway

like familial hypercholesterolemia^{2,3} -the study of which established the field of endocytosis-, Alzheimer's⁵, and some types of cancer⁶. The importance of the endocytic machinery as the entry portal of the cell is evident in the fact that it is hijacked by pathogens like viruses and bacteria to enter host cells⁷. Other components of the cellular signaling pathway transmit signals across the cell and between various organelles like the Golgi apparatus and endoplasmic reticulum. These membranes undergo similar transitions of the bounding membrane, and have mechanistic and biochemical similarities^{8,9}.



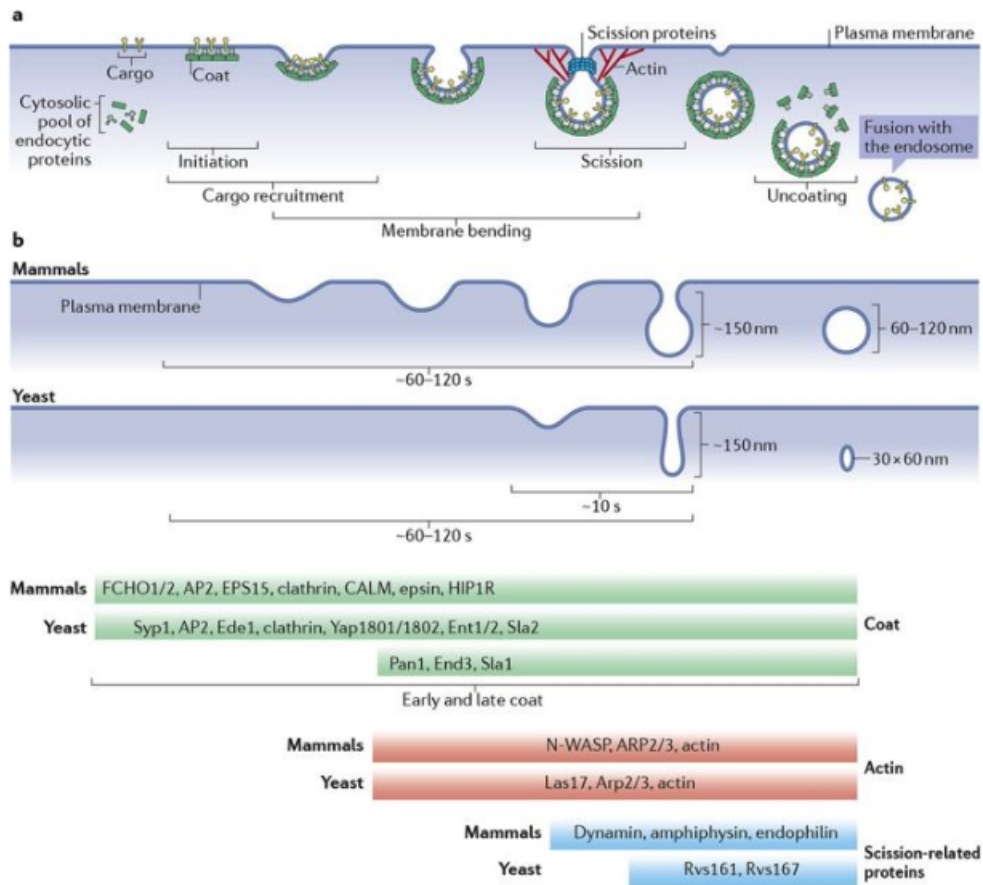
Although many early discoveries relating to endocytic pathways were identified in mammalian cell types^{10,11}, description of endocytosis in *S.cerevisiae*¹² marked the beginning of important findings that were made in the yeast and later verified in mammalian cells. The ease of genetic manipulation, availability of the completed sequence of the yeast genome, and relative simplicity of endocytic pathways-there is only one- drove several discoveries that established yeast as a powerful model organism^{13,14}.

1.2 Clathrin-mediated endocytosis

Many different endocytic pathways that facilitate the internalization of cargo at the plasma membrane exist, as depicted in Fig.2, all differing in the size and type of cargo. Of them, Clathrin-mediated endocytosis (CME), is universal among eukaryotes and contributes to 90% of cargo trafficked into the cell¹⁵. First identified by studying yolk uptake in mosquitos, ultrastructural studies of their oocytes (where the concentration of uptake events is high enough to be easily studied) identified a bristly coat formation on the cell membrane

and similarly bristly vesicles, that then lost this coat and fused to eventually form yolk bodies in the mature oocyte¹⁶. The bristle was noted in several cell types, and was later identified as a lattice of a single highly conserved protein¹⁷. This protein was named Clathrin, derived from the latin word for lattice. Clathrin is formed of light and heavy chains incorporated into a triskelion¹⁸ that assembles into closed hexagonal and pentagonal structures on the inner leaflet of the plasma membrane. Clathrin-mediated endocytosis has, since four decades ago, been recognized has an ubiquitous mechanism of membrane uptake in cell types ranging from the frog presynaptic membrane¹⁹ to rat vas deferens²⁰.

Clathrin and associated proteins do not only interact with the plasma membrane. It has also been observed localizing to the trans-golgi network (TGN); these clathrin-coated vesicles mediate traffic from the TGN to the endosome. Specification of vesicle target to different cellular compartments is achieved by Clathrin interaction with specialized adaptor proteins like the adaptor protein complexes (AP), which specify Golgi-to-early endosome traffic, while Golgi-localized gamma-adaptin (GGA) complexes specify Golgi-to-late endosome traffic. These membrane associations, among others form components of the cellular signaling pathway that transmit signals across the cell and between various organelles like the Golgi apparatus and endoplasmic reticulum. These membranes undergo similar transitions of the bounding membrane, and have some mechanistic and biochemical similarities^{13,14}.



1.3 CME in mammalian and yeast cells

1.3.1 Clathrin is required for mammalian CME

That the clathrin lattice is responsible for remodeling the plasma membrane and selecting cargo was speculated in the first papers that noted the “bristly” coat^{16,21}. In multicellular organisms like *C.elegans*, clathrin depleted by RNAi results in decreased endocytic uptake in oocytes and dead progeny²², in *D.melanogaster*, deletion of clathrin heavy chain results in embryonic lethality²³. In HeLa cells, knock-down of the heavy chain by RNAi results in decrease in endocytosis by 80%²⁴; essentially, endocytosis fails in the absence of clathrin. The exact contribution of clathrin in the progression of endocytosis has been heavily debated, but its involvement itself has not. Although several genes involved in CME in yeast were found to be homologues of the mammalian machinery, however, early work in yeast revealed that clathrin is not necessary for endocytosis²⁵. Loss

of clathrin changes the size of the vesicles formed at scission, and leads to decrease in the number of established endocytic sites^{26,27}: it appears to affect establishment of sites and regulation of scission. It became apparent that though the mammalian and yeast systems were mechanistically similar and most of the yeast endocytic proteins had mammalian homologues²⁸, there are some significant differences.

1.3.2 Actin forces are required for yeast CME

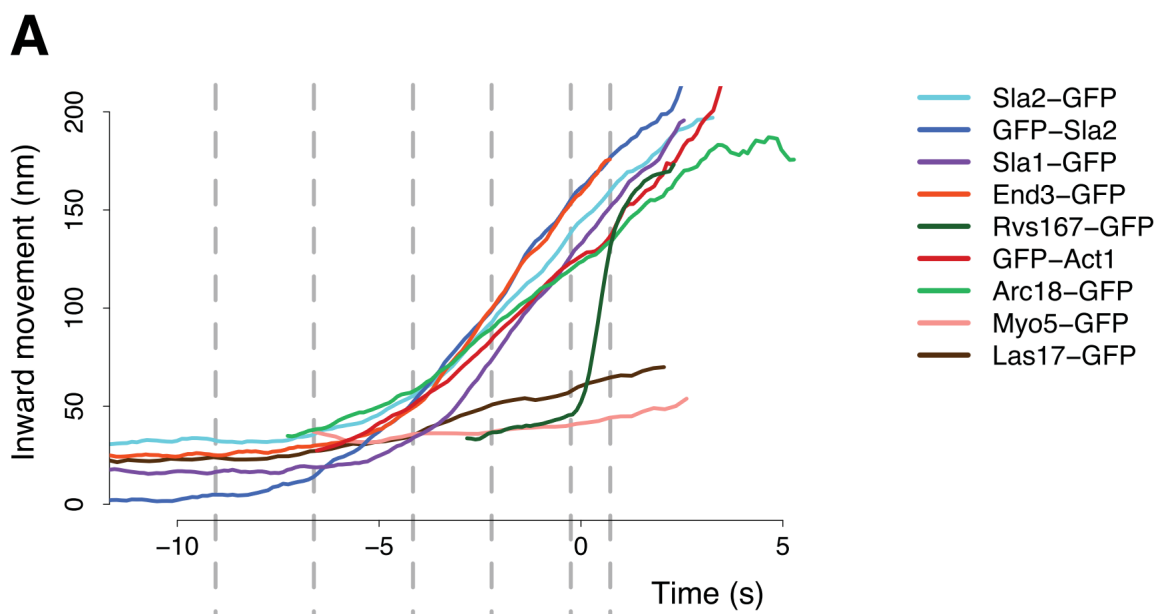
Cortical actin patches were first seen in *S.cerevisiae*, that were later established as endocytic sites from the colocalization of other endocytic proteins. While the mammalian CME uptake is heavily dependent on clathrin, the yeast system relies on actin and its proper organization for endocytosis²⁹. Not only is actin itself necessary for the initiation of plasma membrane deformation³⁰, coupling the endocytic coat to actin are necessary for internalization^{31,32}. The cell wall surrounding the plasma membrane in yeast cells induces a high intracellular turgor pressure³³, which could explain the high force requirement for membrane deformation in yeast.

1.3.3 CME in yeast is highly regular

In yeast, over fifty proteins are recruited, interact, and disassembly during this process. In mammals as well as in yeast, the proteins that arrive at an endocytic site can be distributed into different modules according to their relative time of recruitment and function. A variable initiation phase assembles coat proteins on the plasma membrane and establishes an endocytic site. While the later proteins show relatively high variability in both recruitment as well as time spent at sites in mammalian cells, in yeast this initiation is followed by a very stereotypic sequence of events that assembles coat proteins, nucleates actin, organizes the actin network, invaginates a membrane tube, and finally severs the membrane to produce cargo-filled vesicles²⁶. Coat proteins arrive upon initiation of endocytic sites, the actin and WASP modules arrive next, and includes actin nucleating proteins, actin, actin-binding proteins that organize the actin network and produce forces that begin to pull the membrane into the cytoplasm. The

scission module arrives last, and regulates the final shape transitions of the endocytic site from tubular membrane to vesicle.

Stereotypicity of the post-initiation stages of yeast endocytosis has allowed averaging the behavior of various proteins from multiple endocytic events. Tracking and averaging the behavior of these proteins has led to understanding the spatial and temporal regulation of endocytosis in remarkable detail^{26,34,35}. The multiple stages of endocytosis are discussed below.



1.3.3.1 Early initiation phase

A variable initiation phase establishes endocytic sites and selects cargo³⁶. The earliest proteins to arrive at sites, Ede1 and Syp1 are not required to form endocytic sites. Deletion of an entire seven protein set of early endocytic proteins (Ede1, Syp1, Yap1801/1802, Apl1, Pal1, Pal2) does not prevent endocytosis. It seems that the initiation of endocytosis in yeast is independent of the recruitment of any one protein, and is likely a result of several different cooperative or independent factors³⁶, that could give the process robustness in the absence of alternate pathways for uptake of essential nutrients and signals. The variability in this phase could also provide a “checkpoint”, to ensure that sufficient cargo is loaded²⁸ before later (energy consuming) phases are triggered.

1.3.3.2 Coat module

Coat proteins serve to template later proteins³⁵, as well as form the link between the actin module³², ingressing membrane, and cargo associated with it. Unlike in mammalian cells, as mentioned earlier, clathrin adaptors and the clathrin triskeleon are not necessary for the progression of sites, although deletion of clathrin introduces a high variability in the timing of scission²⁷.

Deletion of coat proteins Sla2 and Ent1 results in a particular phenotype in which actin polymerization is achieved, but the membrane is decoupled from actin forces, resulting in actin “flames” without membrane bending^{32,37}. The complex between proteins Sla1, Pan1 and End3 links the early coat to other coat proteins and polymerized actin, is involved in actin regulation itself, and connects vesicles to actin cables and endosomes^{38–40}. The arrival of Sla1 is a strong predictor of successful endocytosis^{26,41}. These coat proteins are pulled upwards into the cytoplasm, and follow the moving membrane.

1.3.3.3 Actin module

Once the coat proteins are assembled, proteins that nucleate and organize the actin machinery are recruited. Actin filaments are nucleated by the Arp2/3 complex, and act in concert with other actin nucleation promoting factors (NPFs), such as the yeast WASP homologue Las17, type 1 myosins Myo3 and Myo5, Pan1, and actin binding protein Abp1. Apart from Pan1, which moves inwards upon membrane movement and forms part of the coat module, the remaining NPFs are recruited to the base of endocytic sites and do not move inwards with the membrane³⁴. Las17 is a potent actin nucleator, without which endocytosis essentially fails⁴². Myo3/5 are non-processive motors that interact with and can translocate actin filaments, but whose mechanistic contribution is unknown. Deletion of either Myo5 or Myo3 has subtle phenotypes, but deletion of both effectively blocked endocytosis⁴². Abp1 binds actin filaments and activates the Arp2/3 complex.

Bbc1, F-BAR protein Bzz1, and Vrp1 are other actin associated proteins that are recruited within the actin module. Bbc1 is known to inhibit Las17 NPF activity, its deletion accumulates actin at endocytic sites⁴³. Bzz1 relieves Las17 of NPF activity inhibition by Sla142. Vrp1 stimulates the Arp2/3 complex, recruits myosins, and interacts with Las17^{44,45}.

Once NPFs and WASP/Myo proteins are recruited, Arp2/3 is recruited and actin polymerization begins. Along with Arp2/3, actin crosslinkers like Sac6 and Scp1, capping protein complexes like Cap1/Cap2, Aip1/Cofilin, Abp1/Aim3 are recruited. This begins the invagination of membrane, along with the coat proteins. Actin monomers are added at the base of the invagination, and coupled into the membrane via coat proteins, so as actin polymerization progresses, the entire actin network is pushed upwards, taking the membrane along with it³⁴.

1.3.3.4 Scission module

While the role of the yeast dynamin-like Vps1 is unclear, relatively few copies of the Rvs complex are recruited in a time window that spans only a few seconds, and membrane scission occurs when the invagination is about 140nm long, indicating tight regulation of this transition^{30,34}. Coat proteins and the actin network are rapidly disassembled by phosphorylation and dephosphorylation of the components. What actually regulates scission in yeast is not yet determined (see 1.3.5).

1.3.4 Membrane scission in mammalian cells

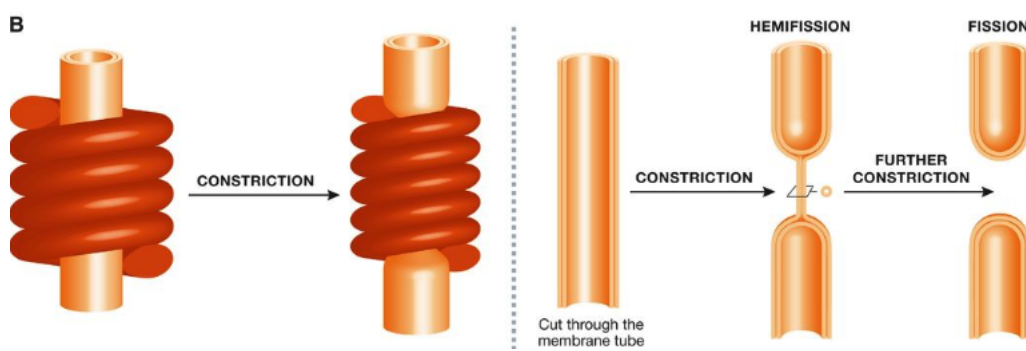
1.3.4.1 Scission is dependent on dynamin

In mammalian cells, membrane scission in endocytosis is primarily effected by the GTPase dynamin. Dynamin was discovered as a microtubule interacting protein⁴⁶, and since has been shown to have a pivotal role in membrane scission and fission at many different organelles across the cell. The importance of dynamin in endocytosis was demonstrated in a temperature sensitive mutant of the Drosophila shibire gene, which results in paralysis of flies at the non-permissive

temperature. These flies fail to form synaptic vesicles 47–49. Shibire codes multiple isoforms of dynamin that are differentially expressed across the organism 50. Knock-down of dynamin isoforms results in initiation of clathrin-coated pits, but vesicle formation is disrupted, resulting in accumulation of a large number of long membrane tubes 51.

1.3.4.2 Dynamin is an oligomeric GTPase

Dynamins consist of a GTPase domain, a stalk region, a bundle signalling element that acts as the linker between the GTPase domain and stalk, a PIP2-binding pleckstrin homology domain (PH) domain and a proline rich domain (PRD) that extends beyond the GTPase domain⁵². In-vitro, dynamin oligomerizes into helical structures with the PH domain apposed against the membrane, and the GTPase domain facing away from the membrane 53,54. Dynamin within the helical structure undergoes conformation changes upon GTP hydrolysis that constricts the helix as well as the membrane tube under it, collapsing the inner leaflet of the bilayer membrane into a hemifused state, resulting in membrane fission⁵⁵. Disruption of its GTPase activity results in membrane tubes that accumulate dynamin, as well as the BAR domain proteins endophilin and amphiphysin^{56–58}



1.3.4.3 Dynamin interacts with BAR proteins to cause scission

Dynamin arrives at clathrin-coated pits via interaction with BAR proteins endophilin and amphiphysin⁵¹. BAR domain proteins form intrinsically curved protein dimers named for the conserved module contained in their founding members, metazoan BIN/ Amphiphysin and yeast proteins Rvs167, Rvs161. In addition to the BAR domain,

most BAR proteins have additional motifs that mediate their interaction with membranes or other proteins: some BAR proteins have an N-terminal amphiphatic helix (N-helix) that is inserted into the membrane, phosphoinositide binding motifs like phox or pleckstrin homology (PH) domains direct BAR proteins to specific lipids within membranes, some BAR proteins have Src homology 3 (SH3) domains that mediate protein-protein interaction. These SH3 regions act as a scaffold for the proline-rich domains of dynamin 59.

1.3.4.4 Dynamin and BAR proteins interact via PRD and SH3 regions

Dynamin's PRD interacts with the SH3 domains of BAR proteins endophilin and amphiphysin59–62. Endophilin recruitment is reduced in the absence of dynamin, and appears to inhibit the GTPase action of dynamin^{60,62,63}, while dynamin recruitment is decreased without endophilin. Amphiphysin levels are unchanged in absence of dynamin, while deletion of amphiphysin results in increased recruitment and prolonged lifetimes of dynamin and absence of membrane scission⁶⁰. These results suggest a role for amphiphysin for disassembly of dynamin involving GTP hydrolysis, and a role for endophilin in dynamin assembly, although the mechanistic interplay between the two BAR proteins with dynamin is still debated, and the sequence of events is not clear^{63,64}. Dynamin localization to localize to clathrin-coated pits is not dependent on BAR proteins, but both GTP hydrolysis and interaction with BAR proteins is necessary for efficient vesicle scission^{60,65}.

1.3.5 Membrane scission in yeast

1.3.5.1 Yeast dynamin-like proteins

In yeast, three dynamin-like large GTPases have been identified: Vps1, Dnm1, and Mgm1. Dnm1 and Mgm1 are involved in mitochondrial fission and fusion⁶⁶. Vps1 is essential for vacuolar protein sorting⁶⁷, is involved in fission and fusion of vacuoles⁶⁸ and peroxisomes⁶⁹, is required for regulation of golgi to endosomal trafficking⁷⁰, and may arrive at early endocytic events⁷¹. None of the three yeast dynamins

have the typical PH domain^{72,73} that in mammalian interacts with the lipid bilayer. Instead, an “InsertB” region likely performs the same function. Although yeast dynamins also do not have PRDs that could interact with the SH3 domains of yeast BAR proteins, Vps1 has been shown to interact with the clathrin and other endocytic proteins^{71,74,75}, though other work has failed to observe localization of Vps1 at endocytic sites^{41,74}. The role of Vps1 in endocytosis is not clear, but it is a candidate for the role of the canonical dynamin in CME.

1.3.5.2 Yeast BAR domain proteins Rvs161/167 regulate scission timing

In yeast, the Amphiphysin/ Endophilin homologue is the heterodimeric complex Rvs161/167⁷⁶ (Rvs), of which Rvs167 has an SH3 domain. Rvs arrives at endocytic sites in the last stage of the endocytosis, and disassembles rapidly at the time of membrane scission³⁴. Deletion of Rvs results in failure of membrane scission in nearly 30% of endocytic events²⁶. Scission failure is identified by the movement inwards of the plasma membrane into the cytoplasm, followed by its retraction back towards the cell wall, indicating a failure to form vesicles. No mutation of known endocytic proteins exhibits this phenotype, while some mutations like that of the yeast Syndapin Bzz1 and Synaptjanin Inp52, in the background of *rvsΔ*, exacerbates the retraction phenotype⁴¹. This unique profile suggests that although Rvs is not necessary for scission, localization of the complex makes scission more efficient, and Rvs likely acts in concert with other proteins to effect this efficiency.

1.3.5.3 What causes scission?

How Rvs may affect scission has not been determined. Since yeast dynamins do not have a PRD, there is likely no interaction with Rvs, so a mechanism that does not involve PRD-SH3 interactions like in mammalian cells is likely necessary. Yeast cells are under high turgor pressure that makes forces from actin polymerization necessary for invagination^{77,78}. There is therefore likely to be some interplay between scission-stage proteins and the actin network that could modulate the final shape transitions.

Proposed scission mechanisms

Several scission models have been presented in the literature so far. Yeast dynamin is the obvious solution to membrane scission. Although none of the three dynamin-like proteins has a proline-rich domain, Vps1 has been suggested to play a role in endocytosis⁷¹. *vps1Δ rvs167Δ* double mutant has been shown to increase membrane retraction rates after invagination⁷⁹, an indication of scission failure. Another hypothesis has proposed that lipid hydrolysis by yeast synaptojanin-like proteins can cause vesicle scission⁸⁰. Synaptojanins dephosphorylate PIP2, a lipid subtype enriched at endocytic sites. In this model, Rvs would form a scaffold on the membrane tube, protecting the underlying PIP2 and causing a boundary between BAR-protected PIP2 at the tube and hydrolyzed PIP2 at the bud tip. This lipid boundary produces a line tension at the interphase that could generate enough force to pinch off a vesicle.

In-vitro experiments have proposed protein friction as a mechanism by which membrane scission could occur⁸¹. In this model, a BAR domain scaffold exerts a frictional force on a membrane that is pulled under it. Such a friction-dependent membrane scission model would predict that if more BAR proteins are added to the membrane, frictional force would increase, and scission should occur at shorter invagination lengths. *In-vivo*, this pulling force is generated by actin polymerization.

Recently, steric pressure exerted on the membrane by disordered protein domains that typically follow the BAR region has been proposed as a mechanism for scission⁸². In these experiments, the amphiphysin BAR domain is able to drive scission, but scission efficiency increases three to four-fold because of the disordered protein domains, and these domains do not need to have any specific biochemical properties: they can be replaced by any other disordered protein region. It has also been proposed that BAR domain scaffold membrane tubes and stabilize them, preventing scission^{83,84}. For a more detailed discussion on these models, see /refresults

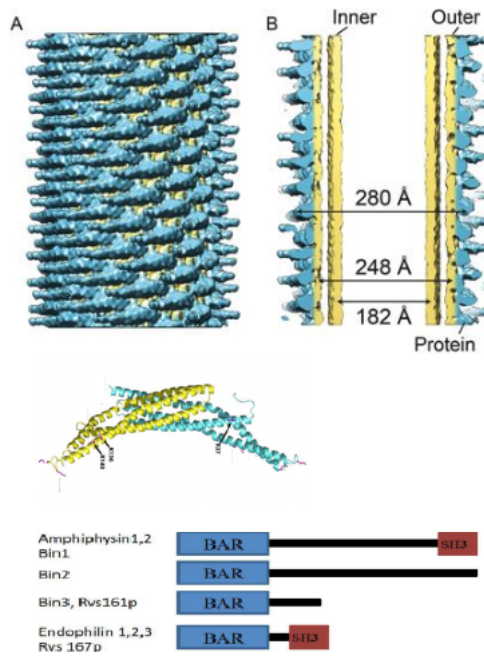
Many of these theories are contradictory, based on in-vitro data, using

mammalian BAR proteins, at concentrations of protein orders of magnitude higher than physiological levels, and without the context of interaction partners, relevant membrane tension, native lipid composition and intra-cellular turgor pressure: a mechanism for membrane scission in yeast is yet to be determined.

1.4 BAR domain proteins

The BAR protein superfamily have a highly conserved BAR domain structure across eukaryotes and are involved in a range of cellular processes including endocytosis, actin organization, cell polarity, transcription and tumor suppression^{85,86}. Of the mammalian isoforms of the founding members, Bin1 (Amphiphysin II) and Bin3 are ubiquitously expressed, while Amphiphysin I is expressed only in neurons. The conserved portion of these proteins, as well as of Rvs167 and Rvs161, is an N-terminal region that forms the BAR domain. This domain typically forms dimers with other BAR domains, and have an intrinsic curvature defined by the dimerization angle. This curvature categorizes BAR proteins to classical BAR, Fer–Cip4-homology-BAR (F-BAR, shallow curvature), and I-BAR (inverted curvature). Membrane-binding is mediated by cationic clusters that bind via non-specific electrostatic interactions to anionic lipids like phosphatidyl serine (PS) or phosphatidylinositol (4,5)-bisphosphate (PtdIns(4,5)P₂ , henceforth PIP₂).

BAR dimers are able to oligomerize and scaffold large areas of membrane. These scaffolds can tubulate and generate curvature across membrane regions much larger than the dimensions of a BAR dimer^{62,87}. BAR scaffolds can also bind membranes in a curvature-dependent manner. Correlation between the membrane shapes that they bind in-vivo and their intrinsic curvature has been shown for many BAR proteins: they may induce, stabilize, or generate specific curvature within cells.



1.4.1 NBAR proteins and membrane shapes

Classical BAR domain proteins form a crescent-shaped structure. Some of them have an N-terminal amphipathic helix (N-helix), forming a subclass of classical BAR called NBAR domains. The two significant endocytic BAR proteins, Endophilins and Amphiphysins, are NBAR proteins. The 35-40 residue N-helix acts as an amphipathic wedge that is unstructured until it is inserted into the upper leaflet of a membrane bilayer 87. The insertion causes displacement of lipids, resulting in bending of the membrane, indicating that N-helix insertion into a membrane bilayer could favor membrane scission both energetically and kinetically 84,88. BAR domains lacking this helix are not able to efficiently tubulate vesicles⁸⁹. The N-helix also increases efficiency of binding to liposomes⁶² in a curvature sensitive manner, and confers salt sensitivity⁸⁹.

High resolution structural data has shown that NBAR proteins can hold form helical scaffolds on tubular membranes 87,90,91. An energetically favorable arrangement of BAR domains consist of dimers parallel to each other, apposed to the membrane, supporting membrane tubulation and preventing scission by stabilizing the membrane tube⁸⁴. Hybrid N-helix and BAR scaffolds can therefore allow coexistence of both vesicles and tubules, with preference for one or the

other depending on the ratio between number of N-helices that favor vesiculation, and BAR generated scaffold stability 84.

Both BAR proteins implicated in CME, Amphiphysin and Endophilin are shown to tubulate membranes in-vitro^{87,89,91} and form a helical scaffold. The tubulation diameter resembles the diameter of the proteins themselves, and involve lateral interactions of the neighboring BAR domains⁹². Both BAR domains are able to form mixed helices in the presence of dynamin^{62,93}.

1.4.2 NBAR protein in endocytosis: Amphiphysin

Two mammalian isoforms of Amphiphysins (Amph) are found. AmphI is enriched in neurons in mammals, while AmphII (Bin1) is expressed in other tissue types, with one isoform enriched in muscle T-tubule junctions⁹⁴. The only Amphiphysin (d-Amph) in flies is expressed in various tissues, and enriched at muscle T-tubule junctions in flies. The d-Amph dimer forms a coiled coil, with each BAR domain made of three long, kinked alpha-helices⁸⁷. In-vitro, liposome tubulation activity of Amphiphysin is concentration dependent, at very high concentrations, it is also able to sever tubular membrane to form vesicles⁸⁷.

Amph I and II both have BAR domains, a proline rich region, and C-terminal SH3 domain. Amphiphysin I, but likely not II binds Clathrin and its adaptors⁹⁵ and can polymerize clathrin into invaginated lattices in a BAR domain dependent manner⁸⁷, while both bind dynamin, and the lipid phosphatase Synaptosomal-associated protein of 61 kDa (Synaptosomal-associated protein 61)⁶¹.

1.4.3 NBAR protein in endocytosis: Endophilin

Endophilins A1-A3 (EndoA) were discovered as SH3 domain containing proteins 96 that co-localized with dynamin, and interacted with Synaptosomal-associated protein 58 and amphiphysin 97: all already identified as important regulators of synaptic vesicle recycling by endocytosis. A second mammalian protein was later discovered as related, and then

termed EndophilinB (EndoB). Other sequenced eukaryotes have a single isoform of EndoA and B.

EndoA1-3 isoforms are found in neurons, ubiquitously, and enriched in the brain and testes respectively. All three are found at presynaptic membranes. Crystal structure of EndoA1 shows essentially the same structure as that of amphiphysin, with an additional amphiphatic helix similar to the N-helix, located at the centre of the crescent-shaped dimer^{89,98}. This helix is thought to insert into the membrane in the same way as the N-helix, potentially inducing faster tubulation of membranes. EndoA1 and 2 may interact with calcium channels at synapses, and may be involved in lipid modification^{99,100}, suggesting different roles for the two BAR domain proteins in membrane interaction. Endophilin interacts with dynamin, NWASP and Synaptojanin proteins via its SH3 domain^{61,63,101}

1.4.4 NBAR protein in yeast endocytosis: the Rvs complex

RVS167 and RVS161 (reduced viability upon starvation) genes were discovered in a screen that tested for survival under starvation conditions¹⁰². Rvs167 and Rvs161 are both NBAR domain proteins that thought to form obligate heterodimeric complexes (Rvs) *in-vivo*^{103,104}. Although there is evidence of heterodimerization: loss of one destabilizes the other, deletion phenotypes of Rvs167 is the same as that of Rvs161, and FCCS measurements indicate that they dimerize^{26,103,105}, it has also been reported that Rvs161 has some functions that do not match that of Rvs167. Rvs161 for instance, interacts with Fus2 in cell-cell fusion, while Rvs167 does not¹⁰⁶. It is consistent however, that at endocytic sites they function together as heterodimers.

Rvs161 and Rvs167 are similar in structure at the N-terminus, both contain NBAR domains that are 42% similar, and although share 21% identity, are not interchangeable¹⁰⁷. In addition to the BAR domain, Rvs167 has a Glycine-Proline-Alanine rich (GPA) region and a C-terminal SH3 region. The GPA region is thought to act as a

linker with no known other function, while loss of the SH3 domain affects budding pattern and actin morphology. Most Rvs deletion phenotypes can however, be recapitulated by expression of the BAR domain alone¹⁰⁴, suggesting that the BAR domains are the main functional unit of the complex.

Deletion of the genes show abnormal actin morphology, confer salt sensitivity, as well as amino-acid and lipid sensitivity, and have abnormal budding pattern^{103,108–110}. Homology modelling has shown that the BAR domain of Rvs167 is similar to Amphiphysin and Endophilin, and is therefore also likely to function similarly to the mammalian homologues. In keeping with this theory, Rvs has been shown to tubulate liposomes in-vitro¹¹¹.

Averaged centroid tracking of the Rvs complex has shown that Rvs arrives in the scission stage of endocytosis. When maximum number of Rvs is recruited, that is, at peak fluorescent intensity, the centroid jumps inwards, concomitant with a sharp decay in fluorescent intensity. This behavior is unique among endocytic proteins, and since similarity in structure with Amphiphysin/ Endophilin BAR domains is expected, has led to the proposition that Rvs may also form a helical scaffold on the membrane tube, whose sudden disassembly either leads to or is caused by membrane scission. The sharp movement into the cytoplasm of the Rvs centroid is then caused by the disassembly of the scaffold, and a jump in the centroid position to the remaining Rvs on the base of the newly formed vesicle³⁴. How Rvs is recruited to endocytic sites, and the cause of the scaffold disassembly are not known, and are the major questions addressed in this work.

2 | Aims of the study

More than 50 different proteins are involved in clathrin-mediated endocytosis. At endocytic sites, they assemble into a small, complex and dynamic macromolecular machinery. Although individual components have been identified and well-characterized during decades of research, their structural organization is poorly understood. In my PhD project, I proposed that single-molecule localization based superresolution microscopy provides both the molecular specificity and necessary spatial resolution to study how proteins are arranged *in situ* within the endocytic machinery. More specifically, I addressed the following questions:

- How is Rvs recruited to endocytic sites?

The recently developed technique of localization microscopy critically depends on dense and specific fluorescent labeling of the cellular structure of interest with a dye suitable for localization microscopy. In the first part of my project, I established an optimized sample preparation pipeline to enable high quality dual-color localization microscopy of yeast cells. These efforts are described in section ??.

- How does it regulate scission

3 | Results

3.1 Tracking endocytic proteins in yeast

Sla1 is a late-stage endocytic coat protein. Since the coat moves inwards with the membrane as it invaginates, it serves as a marker for membrane invagination. Sla1 is used throughout this work to track coat movement. In Fig.3.1B, a kymograph of a Sla1-GFP patch at the plasma membrane of a yeast cell shows it arrives at endocytic sites, and after about 15 seconds, moves inwards into the cytoplasm. Actin-binding protein Abp1, which marks the actin network, also shows movement inwards almost as soon as it arrives at endocytic sites. Rvs167, the scission-stage protein, has a relatively short lifetime, and shows a sharp jump into the cytoplasm.

Averaged centroid tracking in live cells, as described in Picco et al. 1, can quantify this movement and dynamics of endocytic. Briefly described, yeast cells expressing fluorescently-tagged endocytic proteins are imaged at the equatorial plane. Since membrane invagination progresses perpendicularly to the plane of the plasma membrane, proteins patches that move inward with membrane invagination do so in the imaging plane. Centroids of a particular protein as it forms patches at endocytic sites are thus tracked in time. Between 40-50 centroids of each protein are averaged. This provides an averaged centroid that can be followed with high spatial and temporal resolution. When different endocytic proteins are simultaneously imaged with the abundant Abp1, Abp1 provides a frame of reference to which all the proteins can be aligned. Averaged centroid tracking, and correlating these centroid movements with membrane shapes

acquired by correlative light and electron microscopy (CLEM) allows us to understand the dynamics of these proteins in the context of shape transitions of the membrane¹.

Correlating CLEM and centroid tracking has shown that Sla1 starts to moves into the cytoplasm concomitant with the arrival of Abp1, and therefore of actin1–3. Sla1 moves inwards along with the membrane and follows it through endocytosis. As inward movement of the coat begins, the Sla1 patch is disassembled, inferred from the decay of the fluorescent intensity of Sla1-GFP¹ (Fig.3.1D,E). Rvs localizes to endocytic patches later in the endocytic timeline, after parallel membrane tubes are formed³. Membrane scission occurs at around 60% of its lifetime at sites³. At the time of scission, the Rvs167-GFP centroid shows a sharp jump into the cytoplasm, while fluorescent intensity shows a sudden decay, a profile that is unique among endocytic proteins^{1,3}. Rvs is proposed to form a scaffold at the membrane tube. At scission time, this scaffold is thought to disassemble, resulting in an inward jump of the Rvs167 centroid to protein localized at the base of the newly formed vesicle. Abp1 intensity peaks at scission time, and consequently drops, indicating disassembly of the actin network upon vesicle formation. At scission time, the Sla1 centroid has moved about 140nm into the cytoplasm. Sla1 centroid can be tracked about 2-3 seconds after scission occurs. This portion of the centroid movement is marked by an increase in noise in fluorescent signal, and corresponds to diffusion of the vesicle after scission.

Averaged centroid tracking as in Picco et al., is used throughout this work to quantify the movement of endocytic proteins. Averaged centroid movement is referred to as “movement”. Unless indicated otherwise, “scission time” in all the centroid movement plots refers to the fluorescent intensity maximum of averaged Abp1 patches.

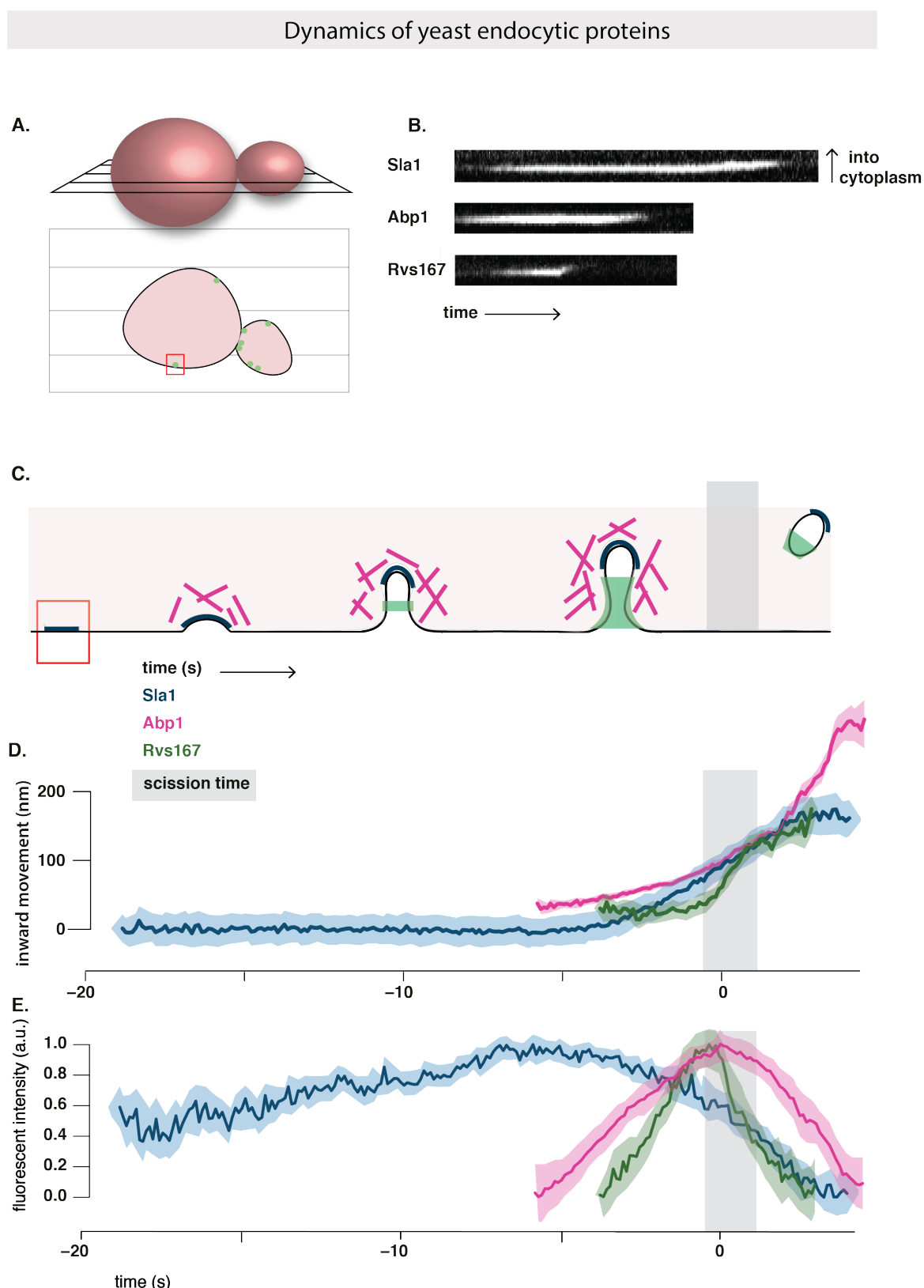


Figure 3.1 – A: Above, schematic of a yeast cell, showing the equatorial plane. Below, cross section of the cell at the equatorial plane, with fluorescently-tagged endocytic protein at the plasma membrane. B: Kymographs of Sla1-GFP, Abp1-GFP and Rvs167-GFP at endocytic sites. Exposure 80ms. C: Schematic of the timeline of membrane invagination during endocytosis, with Sla1, Abp1, Rvs167 and scission time (around 60% of Rvs167 lifetime) indicated. D, E: Averaged centroid movement and normalized fluorescent intensity for GFP-tagged Sla1, Abp1 and Rvs167. D and E are aligned in time so that time=0 (sec) corresponds to the maximum of fluorescent intensity of averaged Abp1 patches. This corresponds to scission time.

3.2 Rvs deletion phenotype

The Rvs complex, as has been discussed in 1, is known to have an influence on membrane scission efficiency. Recruitment in the final stage of membrane invagination, localization to the membrane tube, and disassembly concomitant with scission all indicate that Rvs could mechanistically influence the scission process.

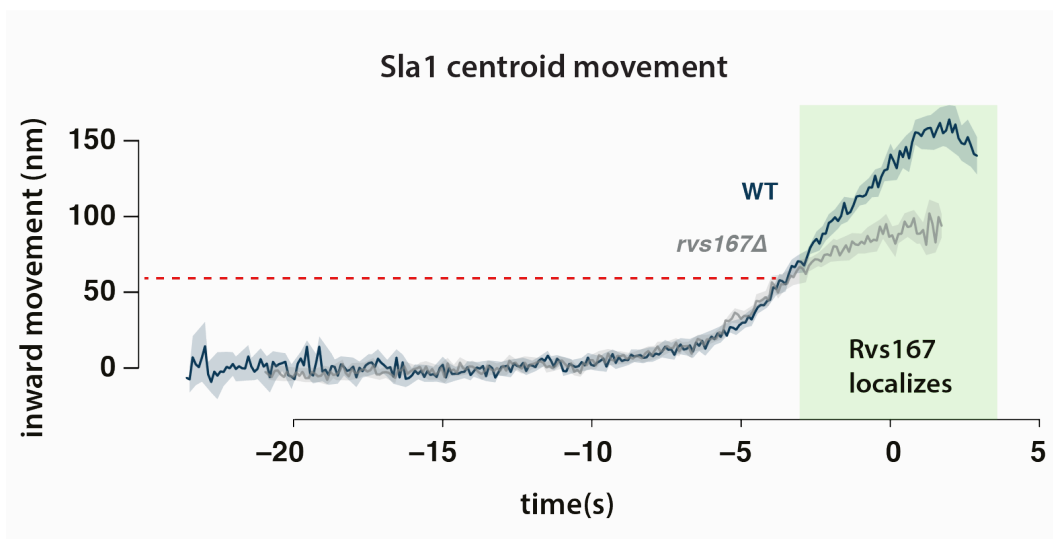


Figure 3.2 – Movement of Sla1 in WT and *rvs167 Δ* cells. WT Sla1 is aligned so that time=0 (sec) corresponds to scission time. Sla1 centroid in *rvs167 Δ* cells is shifted in time so that it moves inwards at the same time as WT Sla1. Red line indicates approximate start of deviation of *rvs167 Δ* from WT.

In order to quantify what happens in the absence of Rvs, I tracked Sla1-GFP in *rvs167 Δ* cells and compared its movement against WT Sla1-GFP movement (Fig.3.2). 27% of Sla1 patches begin to move inward but retract, consistent with earlier observations². Movement of the remaining 73% Sla1 patches are quantified. Sla1 movement of *rvs167*deletion and WT looks similar up to about 60nm. CLEM has shown that Rvs167 localizes to endocytic sites after the tubes are 60nm long. Sla1 movement in *rvs167*deletion shows therefore that membrane invagination is unaffected till Rvs is supposed to arrive. Sla1 in *rvs167 Δ* then continues to move at a much slower rate, and membrane scission occurs at about 80nm. In WT, Sla1 continues to move inwards to 140nm. This indicates that first, membrane scission can occur at invagination lengths of 80nm. Then, that the arrival

of Rvs prevents membrane scission at this point and allows further membrane invagination.

3.3 Recruitment of Rvs and function of domains

Membrane curvature-sensing / generation by BAR proteins Cellular membrane shape is a result of properties like rigidity, tension, intracellular pressure, that are all influenced by membrane lipid composition and the proteins embedded in it 4,5. Since these properties all oppose membrane deformation, energy is required to deform and bend it. BAR domains localize to curved membranes, but they have also been shown to generate membrane tubes and cause vesicle formation, leading to some discussion on the interplay between these functions.

Membrane curvature-sensing / generation by BAR proteins BAR domains are thought to generate membrane curvature by either scaffolding or insertion of the N-helix into the lipid bilayer. Scaffolding refers interaction of the positively charged concave surface of BAR domains with negatively charged lipids. By attracting lipids to the positive surface, BAR domains are thought to induce membrane curvature. Curvature-generation by BAR scaffolding has been proposed as a function for I-BAR, F-BAR as well as N-BAR domains 6–10.

N-helices similar to that of NBAR domains can generate curvature independently of the BAR scaffold mechanism11,12. Shallow insertion of the N-helix into the upper lipid bilayer causes the bilayer to rearrange, and results in a difference in membrane surface area between the upper and lower leaflets13. This results in membrane curvature.

Sensing curvature: BAR domains show preferential binding to membranes that correlates to their intrinsic curvature: flat F-BAR domain

proteins are found at flat membranes, N-BAR domains are found at tubular structures^{1,14}. That BAR domains are able to generate curvature does not imply that this is their function. In-vivo, the significance of curvature-generation is not determined. Tracking over thirty different endocytic proteins in NIH-3TC cells (derived from mouse fibroblasts), TIRF imaging shows that Endophilin2 and Amphiphysin1 arrive late in the endocytic time-line right before scission¹⁵, suggesting they arrive when membrane tubes are already formed.

Curvature-generation and sensing are likely intrinsically coupled mechanisms. BAR proteins that can induce curvature could also sense curvature: there could be feedback between membrane-sensing and generation. In the case of Rvs, that the complex localizes to sites after membrane tubes are formed shows that Rvs localizes once membrane curvature is established. Whether this localization is dependent on membrane curvature, recognized by the BAR domain is not known.

3.3.1 BAR domains sense membrane curvature *in-vivo*

To test whether Rvs is recruited because of membrane curvature, I tested the recruitment of Rvs167 without the BAR domain, that is Rvs167-delsh3 (henceforth BAR. Cells that contain Rvs167 without the SH3 domain are referred to as BAR cells). BAR-GFP forms cortical patches (Fig.3.3A), so the BAR domain is able to localize to the plasma membrane in the absence of the SH3 domain. In yeast cells expressing both BAR-GFP and Abp1-mCherry, BAR-GFP co-localizes with Abp1, indicating that BAR domains are recruited to endocytic patches (Fig.3.3A, C).

In order to test whether this localization is due to membrane curvature, I compared the dynamics of Rvs167-GFP against BAR-GFP in *sla2Δ*cells (Fig.3.3D-F). Sla2 is a coat protein that acts as a linker between the membrane and actin cytoskeleton. It binds membrane via its N-terminal ANTH domain and actin by the C-terminal THATCH domain. This allows forces generated by the actin network to be

transmitted to the membrane¹⁶. In *sla2Δ* cells, rather than cortical actin patches that co-localize to endocytic proteins, an “uncoupling phenotype” is observed^{16,17}. Although endocytic coats are formed, actin is polymerized continuously at these sites, the membrane is not pulled inwards, and vesicles are not formed. Forces generated by the actin network are not transmitted to the membrane (Fig.3.3E).

In *sla2Δ* cells, Rvs167-GFP is recruited to the plasma membrane (Fig.3.3D,F), together with Abp1. Some Rvs167-GFP patches persist at the plasma membrane, while many are assembled and disassembled. In *sla2Δ* cells expressing BAR-GFP, localization is removed except for rare transient patches at the plasma membrane. These patches rarely co-localized with Abp1. Rvs167-GFP and BAR-GFP patches are both dynamic, indicating an interaction exists in both cases that is able to assemble and disassemble Rvs molecules at the plasma membrane.

BAR-GFP is not typically recruited to the plasma membrane in *sla2Δ* cells, showing that the BAR domain requires membrane curvature to localize.

3.3.2 The SH3 domain is able to localize Rvs in an actin and curvature-independent manner

As seen in the previous section 3.3.1, full-length Rvs is able to localize to cortical patches in *sla2Δ* cells. Full-length Rvs167 is able to localize to endocytic patches in *sla2Δ* cells. This localization must be dependent on the SH3 domain, since BAR alone does not localize in *sla2Δ* cells. SH3 domains are known to interact many actin associated proteins: an interaction with Abp1 has been shown, as well as with Las17, type I Myosins, and Vrp1.

In order to test whether it interacts with an actin binding protein, I imaged BAR-GFP and full-length Rvs167-GFP in *sla2Δ* cells treated with the actin sequestering agent LatrunculinA (LatA). LatA is a sea-sponge toxin that binds monomeric actin and prevents incorporation of actin into filaments. Since high actin turnover is required at endocytic sites, LatA effectively disassembles the actin network, and blocks endocytosis. In *sla2Δ* cells treated with LatA, membrane curvature as well as actin-binding proteins are removed from endocytic sites. Loss of actin-binding proteins is observed by the loss of Abp1 signal.

Surprisingly, full-length Rvs167 is transiently localized to the plasma membrane in *sla2Δ* cells with LatA (Fig.3.3G, H). Localization occurs in the absence of a BAR-membrane interaction, since BAR-GFP

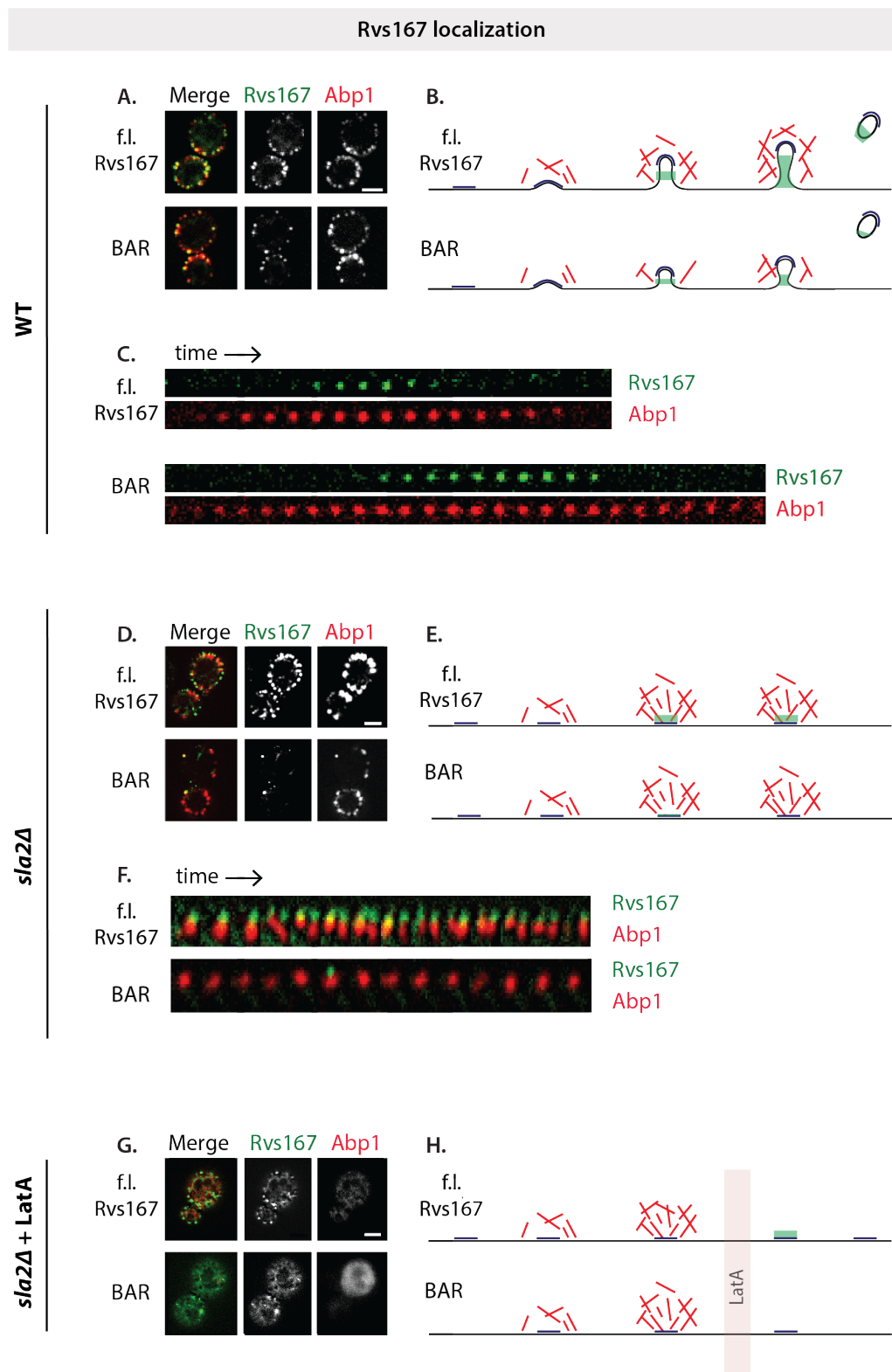


Figure 3.3 – A: Maximum intensity projection of Rvs167-GFP in WT and BAR cells, and Abp1-mCherry. Exposure 250ms. B: Schematic of membrane progression in WT and BAR (see section 3.3.3). C: Montage of Rvs167-GFP in WT and BAR cells, and Abp1-mCherry. Time between frames= 750ms. D: Max. int.projection of Rvs167-GFP and Abp1-mCherry in *sla2Δ* and *sla2Δ*BAR cells, E: Schematic of membrane invagination in *sla2Δ*. F: Montage of Rvs167-GFP and Abp1-mCherry in WT and BAR cells. Exposure 1000ms for GFP, 800ms for RFP. G: Max. int. projection of Rvs167-GFP and Abp1-mCherry in *sla2Δ* and *sla2Δ*BAR cells after treatment with LatA for 10'. Exposure 1000ms for GFP, 800ms for RFP. H: Schematic of membrane invagination in *sla2Δ* cells treated with LatA. All scale bars = 2um.

patches are not seen in similarly treated cells. This suggests that the SH3 domain is able to recruit Rvs to the plasma membrane in the absence of curvature and actin network components. Rvs167-GFP patches are transient, so assembly and disassembly of an Rvs patch can be mediated by the SH3 domain. Localization of Rvs161, which does not have an SH3 domain, is removed by LatA treatment¹⁷, supporting the conclusion that the SH3 domain drives the localization of full-length Rvs167 in *sla2Δ*cells, as well as in *sla2Δ*cells with LatA.

3.3.3 Loss of the SH3 domain affects progression of endocytic sites

The BAR domain was expected to act as the functional module of the Rvs complex: phenotypes of *rvs167Δ*such as non-viability on starvation, and mis-localization of actin can be effectively rescued by expression of the BAR domain alone¹⁸. Since the SH3 domain unexpectedly influences localization of Rvs, I investigated its effect further.

The SH3 domain generally mediates protein-protein interaction by binding to proline-rich sequences that contain a core PXXP motif^{19,20} (where X is any amino acid). These domains are ubiquitous in cellular interaction pathways, and several endocytic proteins have at least one SH3 domain. Although SH3 domains are abundant, they appear to have specific binding partners that could modulate function. For Rvs167, neither binding partner, nor function of the SH3 domain is clear.

In order to probe the contribution of the Rvs SH3 domain to endocytosis, I studied Sla1 and Rvs167 in BAR cells, and quantified the number of molecules recruited to endocytic sites as in Picco et al.,¹. Fig.3.4C shows that recruitment of Rvs167 is reduced by half (57 ± 9.9 for BAR compared to 113.5 ± 5.3 for WT). Cytoplasmic concentration of Rvs167 appears not to be different in WT vs BAR cells (see methods). The inward jump of Rvs167 is reduced in BAR cells compared to WT (Fig.2.3A). Movement of the coat protein Sla1

is similarly reduced (Fig.2.3A). Sla1 moves into the cytoplasm approximately 60nm instead of the 140nm found in WT invaginations. Abp1 recruitment in BAR cells is reduced to 50% of WT recruitment, to 172.6 ± 12.9 from 347 ± 30.6 molecules in WT (Fig.2.3C). Short invaginations with a maximum of 60nm have been observed in the case of Rvs167 deletion by CLEM3, which is about the same length as those observed in the SH3 deletion: loss of the SH3 domain appears to be detrimental to the function of the Rvs complex. That tubular invaginations are formed in BAR cells, and qualitatively resemble that in WT cells is demonstrated by CLEM on WT and BAR samples expressing Rvs167-GFP and Abp1-mCherry (Fig.3.4E).

To check if there was a change in the timing of endocytic progression, I quantified the lifetimes of Rvs167, Sla1 and Abp1 in BAR cells using total internal reflection fluorescence (TIRF) microscopy. Unlike epifluorescence microscopy at the equatorial plane, in TIRF only fluorophores up to a depth of about 100nm from the glass-sample interphase are excited. This reduces fluorescent signal from the cytoplasm, allowing detection of low intensity fluorescent signal, and is a better method for quantification of protein lifetime than epifluorescence microscopy. Although this method is sensitive to low fluorescent intensity, as the proteins start to move inwards into the cytoplasm, fluorescent intensity rapidly drops, because of the limited excitation depth. Therefore, rather than a quantification of the entire lifetime of the protein, this is a quantification of the non-motile lifetime of a protein that arrives at endocytic sites. Non-motile lifetimes of Rvs167, Sla1 and Abp1 are thus compared between BAR and WT cells.

While lifetimes of Rvs167 and Sla1 are similar in both cell types, there is a significant increase in the lifetime of Abp1 in BAR cells (supplemental). Increase in lifetime of Abp1 is also seen by epifluorescence microscopy (Fig.3.4B). I then looked for differences in the sequence of recruitment of these proteins by looking at the difference in time between recruitment of Sla1 and Rvs167, and the difference in time between recruitment of Abp1 and Rvs167. The time difference between recruitment of Sla1 and Rvs167 is unchanged between WT and BAR cells, while the difference in time between recruitment of Abp1 and Rvs167 is increased in BAR cells (Fig.3.4D).

This data suggests that the BAR domain alone cannot reproduce the function of the Rvs167 at endocytic sites: recruitment of Rvs, coat and actin dynamics are all affected.

3.4 Function of Rvs

3.4.1 BAR domains as scaffold for dynamin

Yeast dynamin Vps1 While work on membrane scission in mammalian cells has converged on the idea that it is caused by dynamin interaction with BAR domains, in yeast what causes the final shape-transition from tubes to vesicles is not determined. Several membrane scission mechanisms for yeast endocytosis have been proposed in the last years, in the absence of conclusive mechanistic evidence. We know that Rvs plays a major role in determining the efficiency of membrane scission, and that in its absence membrane invaginations are shorter than in WT. I have therefore focused of models for membrane scission that assign a central role to BAR domain proteins. In the following pages, I discuss their propositions, describe experiments that have tested these mechanisms, and the conclusions they propose.

Rvs as an interaction surface for dynamin

Yeast dynamin is the obvious solution to membrane scission. None of the three dynamin-like yeast proteins has a proline-rich domain that are known to bind BAR domains, but one of them- Vps1 has been suggested to function like the mammalian homologue 21,22. Rooij et al., propose that Vps1 localizes to endocytic sites at scission stage, and see that in $vps1\Delta rvs167\Delta$ cells, rates of coat retraction after invagination increases. Coat retraction after invagination is an indication of membrane scission failure2. Vps1-GFP does not localize to endocytic sites in Gadila et al.,23, but localizes to the golgi body and to vacuoles. Kishimoto et al24, do not find a co-localization between Vps1 and Abp1, and find that the $vps1\Delta rvs167\Delta$ cells do not show increased coat retraction rates. Vps1 tagged with GFP as well as superfolded GFP, and imaged by TIRF microscopy fails to co-localize with Abp1 (data from Andrea Picco, not shown). The

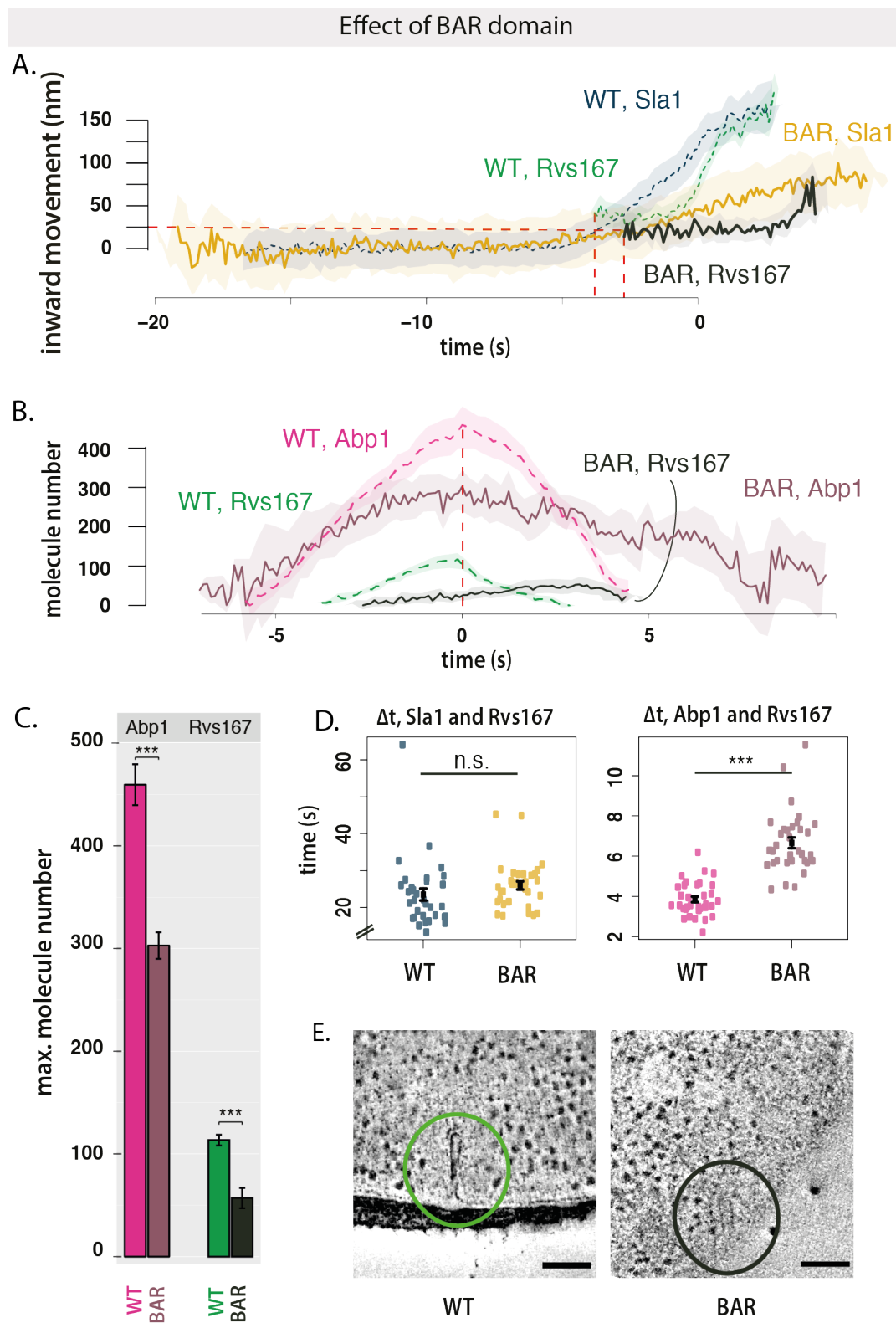


Figure 3.4 – A: Movement of Sla1 and Rvs167 in WT and BAR strains. All centroid movements are aligned so that time=0 (s) corresponds to scission time. **C:** Molecule numbers of Abp1-GFP and Rvs167-GFP in WT and BAR cells. P-values from two-sided z test, * = $p \leq 0.05$, ** = $p \leq 0.01$, *** = $p \leq 0.001$. **D:** Time difference between arrival of Sla1 or Abp1 and Rvs167 in WT and BAR cells. Time difference measured from TIRF images of Rvs167-GFP/ Abp1-mCherry and Rvs167-GFP/ Sla1-mCherry. Mean and standard error of the mean are shown. p values of two-sided t test, * = $p \leq 0.05$, ** = $p \leq 0.01$, *** = $p \leq 0.001$. **E:** Z-stack of slices from reconstructed tomograms of WT and BAR strains expressing Rvs167-GFP and Abp1-mCherry. Scale bar=100nm.

debate concerning the involvement of Vps1 in membrane scission in yeast has been compounded by the possibility that the GFP tag on Vps1 could interfere with its localization to endocytic sites, and/or its interaction with the Rvs complex.

If Vps1 was required for membrane scission, Sla1 would be expected to undergo delayed or failed scission in its absence, and Rvs dynamics would be affected.

3.4.1.1 Vps1 does not affect Sla1 or Rvs167 dynamics

I investigated the role of Vps1 by studying coat and scission proteins in *vps1Δ* cells in order to avoid the question of whether fluorescently tagging Vps1 affects its function.

vps1Δ cells show a slight growth defect at 37°C, as has been reported²¹. In *vps1Δ* cells, Sla1 accumulates in patches at the plasma membrane, moves inwards, and disassembles like in WT. *vps1Δ* does not increase the rate of membrane retraction (Fig.3.5C).

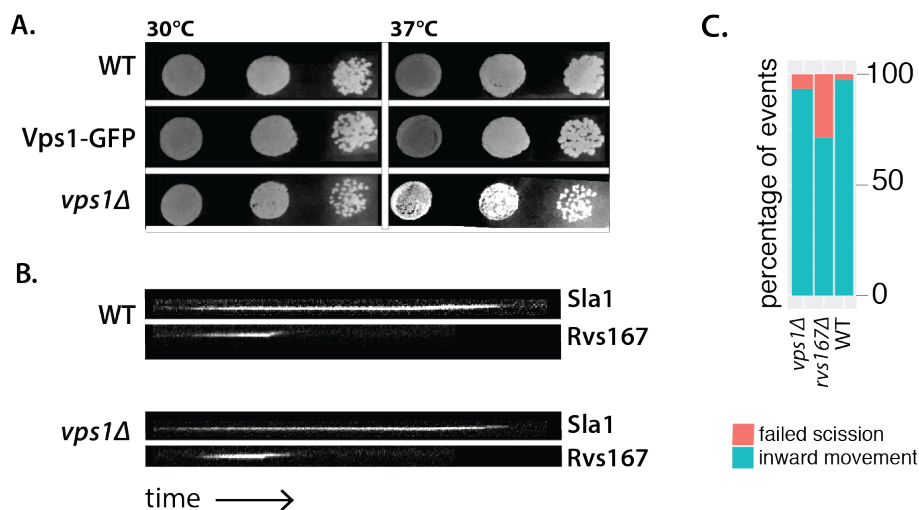


Figure 3.5 – A: Dot spots of yeast cells in WT, Vps1-GFP (diploid), and *vps1Δ* cell at 30°C and 37°C. B: Kymographs of Sla1-GFP and Rvs167-GFP in WT and *vps1Δ* cells. Exposure 80ms. C: Failure rate of membrane scission, in WT, *vps1Δ*, and *rvs167Δ* cells.

Centroid movements and intensities of Sla1 and Rvs167 in time are plotted in Figure 3.6. WT Sla1 is aligned so that time=0 (s) corresponds to scission time. Sla1 movement for *vps1Δ* in Fig.3.6A is shifted in time so that it starts to move inwards at the same time as WT. The lifetime of Sla1-GFP appears to be slightly shortened in *vps1Δ* compared to the WT, but this shortening occurs early in the lifetime of the protein at endocytic patches, when the molecule numbers of

Sla1 are low. Epifluorescence microscopy is not particularly sensitive in this range of fluorescent intensity. Therefore, I do not take this to indicate a true shortened lifetime; lifetime of Sla1 in *vps1Δ* was not investigated further. Similar to WT, Sla1 in *vps1Δ* moves into the cytoplasm about 140nm before membrane scission occurs. Sla1 moves inward at the same rate, and to similar maxima as WT.

Dynamics of Rvs167 also remains the same as in WT (Fig.3.6C, D). Magnitude of centroid movement is unchanged, indicating that the base of the vesicle formed is likely at the same position as in WT. Fluorescent intensity shows the typical sharp drop. This data indicates that if Vps1 is localized to endocytic patches in *S.cerevisiae*, it is not involved in regulating membrane scission.

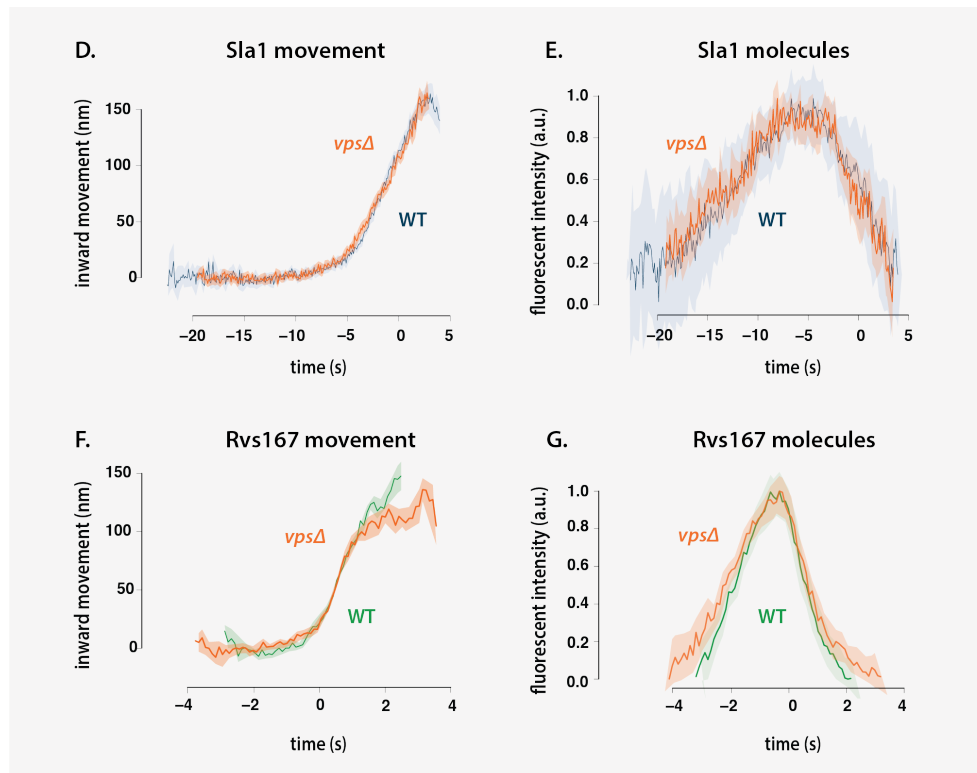


Figure 3.6 – A, B: Movement and normalized fluorescent intensity of Sla1 in WT and *vps1Δ* cells. Time = 0 (s) for WT Sla1 centroid corresponds to scission time. Sla1 centroid for *vps1Δ* is shifted in time to begin inwards movement at the same time as WT. C, D: Movement and normalized fluorescent intensity of Rvs167-GFP in WT and *vps1Δ* cells. Time = 0 (s) for WT Rvs167 centroid corresponds to scission time. Rvs167 for *vps1Δ* is shifted so that fluorescent intensity maxima is at time=0 (s).

**Rvs forms a barrier for lipid diffusion,
generating forces for scission**

Phosphatidylinositol (PIs) and their lipid derivatives play important roles in many cellular processes including membrane trafficking and cell signalling. Conversion between lipid types is driven by kinases, lipases, and phosphatases and controlled throughout the membrane trafficking pathway.

Phosphatidylinositol (4,5)-biphosphate (PI(4,5)P₂) is an important lipid type found at the cell surface, and is enriched and depleted from endocytic sites at the plasma membrane in concert with the assembly and disassembly of the endocytic machinery. Synaptojanins form a subset of inositol polyphosphate 5-phosphatases that hydrolyze PI(4,5)P₂ to PI(4)P by removing the phosphate at the 5' position of the inositol ring. They are known to take part in CME and intracellular signalling, as well as in modulating the actin cytoskeleton²⁵.

In mammalian cells, disruption of Synaptojanin genes results in cellular accumulation of PI(4,5)P₂ at endocytic sites. Coated vesicles gather at the plasma membrane, suggesting a role for lipid hydrolysis in releasing coat proteins from nascent vesicles. Synaptojanins contain an N-terminal homology domain with the cytoplasmic domain of the yeast SAC1 gene that is implicated in lipid metabolism, actin morphology, and vesicle transport in the secretary pathway²⁶. A central catalytic domain is then followed by a proline-rich C-terminal region that is the canonical interaction partner of SH3 domains. Synaptojanins interact with actin binding proteins and BAR domain proteins, potentiating also a role in membrane invagination and scission.

The yeast genome encodes for three Synaptojanin-like proteins- Inp51, Inp52 and Inp53- that regulate phospholipid metabolism. In *inp51Δ* *inp52Δ* cells, increased lifetimes of endocytic proteins and produce aberrant membrane invaginations that could indicate scission failure and defective endocytosis^{27,28}. *inp52Δ rvs167Δ* cells have increase membrane retraction rates, supporting a possible role for Inp52 in membrane scission²⁴. Loss of *inp51* leads to an increase in bulk

PI(4,5)P₂ level. Changes in PI(4,5)P₂ levels have not been reported for mutations of Inp52, and are lipid levels not measured locally at the endocytic sites^{29,30}.

In a model proposed by Liu et al, Synpatojanins and BAR proteins interact to regulate PI(4,5)P₂ hydrolysis, which in turn drives membrane scission. Here, Rvs forms a scaffold on the membrane tube, and protects the underlying PIP₂ from hydrolysis. Synaptojanin arrives at invaginated membranes, and hydrolyses unprotected PIP₂. This generates a boundary between BAR-protected PI(4,5)P₂ at the tube and PI(4,5)P at the bud tip. This lipid boundary produces line tension at the interphase that could generate enough force to pinch off a vesicle. The Liu et al., model predicts that if line-tension from lipid hydrolysis is removed, membrane scission should be delayed or fail.

3.4.2 Yeast synaptojanins do not significantly affect coat and Rvs movement

I tested the lipid hydrolysis model described above by studying the effect of synaptojanin deletion on Sla1 and Rvs167. Of the three yeast Synaptojanins, only Inp52-GFP localizes to cortical patches Fig.3.7A. Time alignment with other endocytic proteins as in Picco et al., shows that Inp52 localizes to endocytic sites at the late stage of scission, similar to Rvs. The centroid of Inp52-GFP can be localized to the tip of the invaginated tube (Fig.2.6D), consistent with the Liu theory of membrane scission: spatial and temporal localization is consistent with influence on scission. Inp51-GFP exhibits a diffuse cytoplasmic signal, while Inp53 localizes to patches within the cytoplasm, likely to the trans-golgi network, as has been noted in other work³¹.

In *inp51Δ* and in *inp52Δ* cells, Sla1-GFP patches are assembled and disassembled, as is Rvs167-GFP. Sla1 retraction rates are slightly increased to 12% in *inp52Δ*, compared to 2% in WT, and 6% in *inp51Δ* (Fig.3.7B).

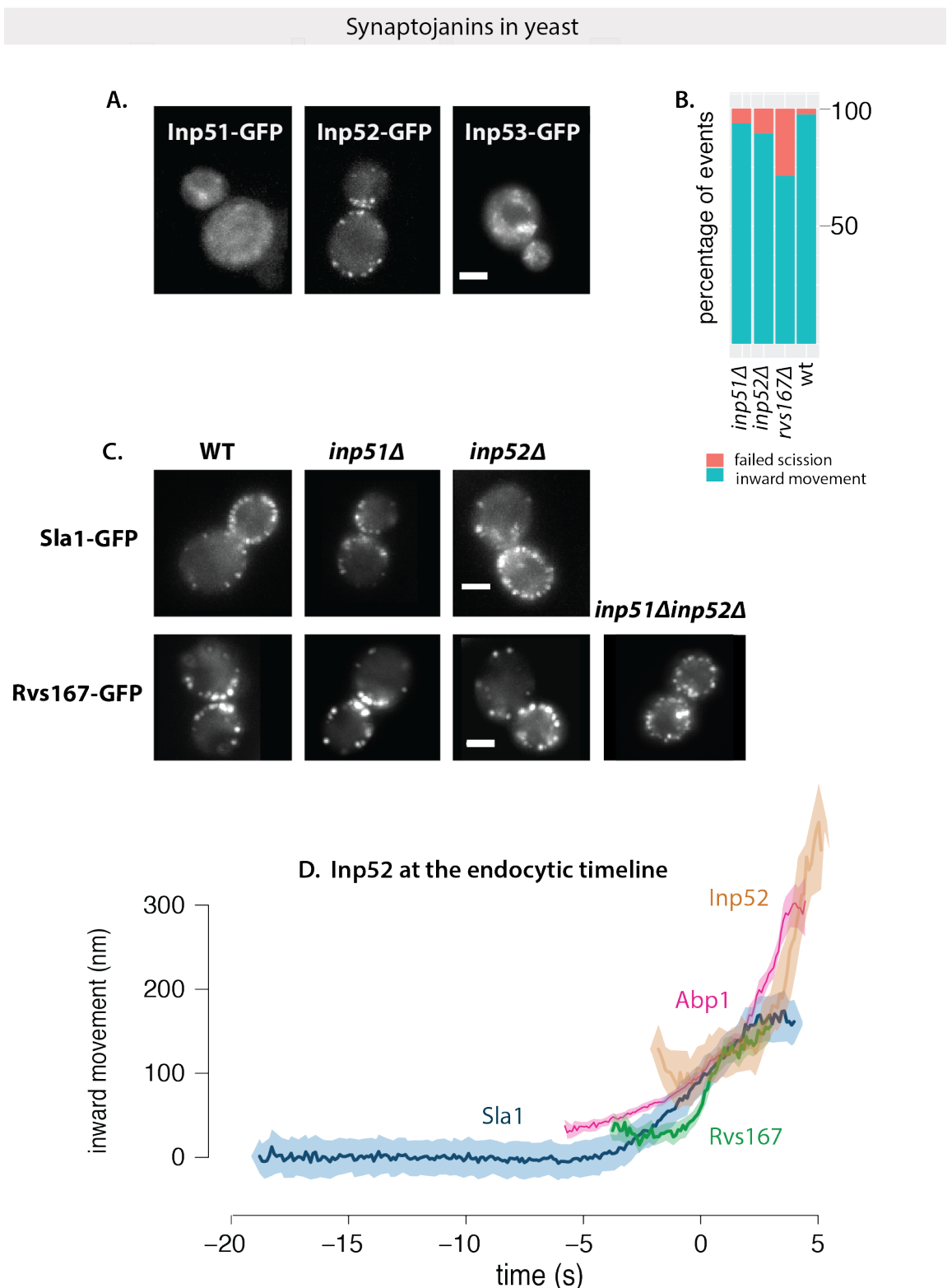


Figure 3.7 – A: Maximum intensity projections of cells expressing GFP-tagged Inp51, Inp52, and Inp53. Exposure time 80ms. B: Failure rate of membrane scission in WT, *rvs167Δ*, *inp51Δ* and *inp52Δ* strains. C: Maximum intensity projection of Sla1-GFP in WT, *inp51Δ*, *inp52Δ* and *inp51Δinp52Δ* cells. Max. int. projection of Rvs167-GFP in WT, *inp51Δ*, *inp52Δ* and *inp51Δinp52Δ* cells. D: Inp52-GFP in endocytic timeline in WT cells. Time=0 (s) is scission time. All scale bars =2um.

In Fig.2.7A, Sla1 movement in $\text{inp}51\Delta$ and $\text{inp}52\Delta$ cells is compared against that in WT. WT Sla1 is aligned in time so that time=0 (s) corresponds to scission time. Sla1 centroids for $\text{inp}51\Delta$ and $\text{inp}52\Delta$ are shifted so that they begin to move inwards at the same time as the WT. All three Sla1 centroids have the same rate of inward movement. While Sla1 in $\text{inp}51\Delta$ moves inwards to about the same distance as WT, in $\text{inp}52\Delta$, the centroid of Sla1 persists for nearly 5 seconds longer than WT (arrowhead in Fig.3.8A). This centroid movement is noisier than the inward movement preceding it, and is likely from post-scission of movement of the vesicle.

Rvs167 dynamics are similar to WT in both $\text{inp}51\Delta$ and $\text{inp}52\Delta$ cells (Fig.3.8C, D). Rvs167 centroids move inwards to about the same distance into the cytoplasm at the jump inwards. In $\text{inp}52\Delta$ cells, however, Rvs167 patches appear to not disassembly completely (arrowhead in Fig.3.8C) unlike in the WT. Since Rvs disassembly occurs at membrane tube scission, this change in Rvs167 dynamics is post-scission. Assembly of Rvs167 in the $\text{inp}51\Delta$ takes about 2 seconds longer compared to WT. The implication of this delay is not thus far clear.

Since the differences in Sla1 and Rvs167 centroid dynamics for $\text{inp}52\Delta$ are post-scission, I find that the data is consistent with a role for Inp52 in removing Sla1 and Rvs167 from vesicles, rather than a primary role in membrane scission.

I then quantified the number of Rvs167 molecules recruited to endocytic patches in $\text{inp}51\Delta$, $\text{inp}52\Delta$, and $\text{inp}51\Delta \text{ inp}52\Delta$ cells. WT levels of Rvs167 are recruited in both $\text{inp}51\Delta$ and $\text{inp}52\Delta$ cases. In $\text{inp}51\Delta \text{ inp}52\Delta$ however, nearly three times as much Rvs is recruited to sites (Fig.3.8B). Some Rvs167-GFP patches in these cells assemble and disassemble, although majority do not. Many large clusters of Rvs167 are present on the plasma membrane, and the regular inward jump in WT is not seen. Some cytoplasmic patches are also seen, consistent with observations of Sla1 patches within the cytoplasm³² by other labs. These patches likely mark aberrant membrane invaginations continuous with the plasma membrane that are able to assemble

and disassemble endocytic patches. Many Sla1 patches are motile in *inp51Δ* *inp52Δ*, and uptake of extracellular membrane appears to proceed in spite of the morphological aberrations. This means that membrane scission could occur in these cells³².

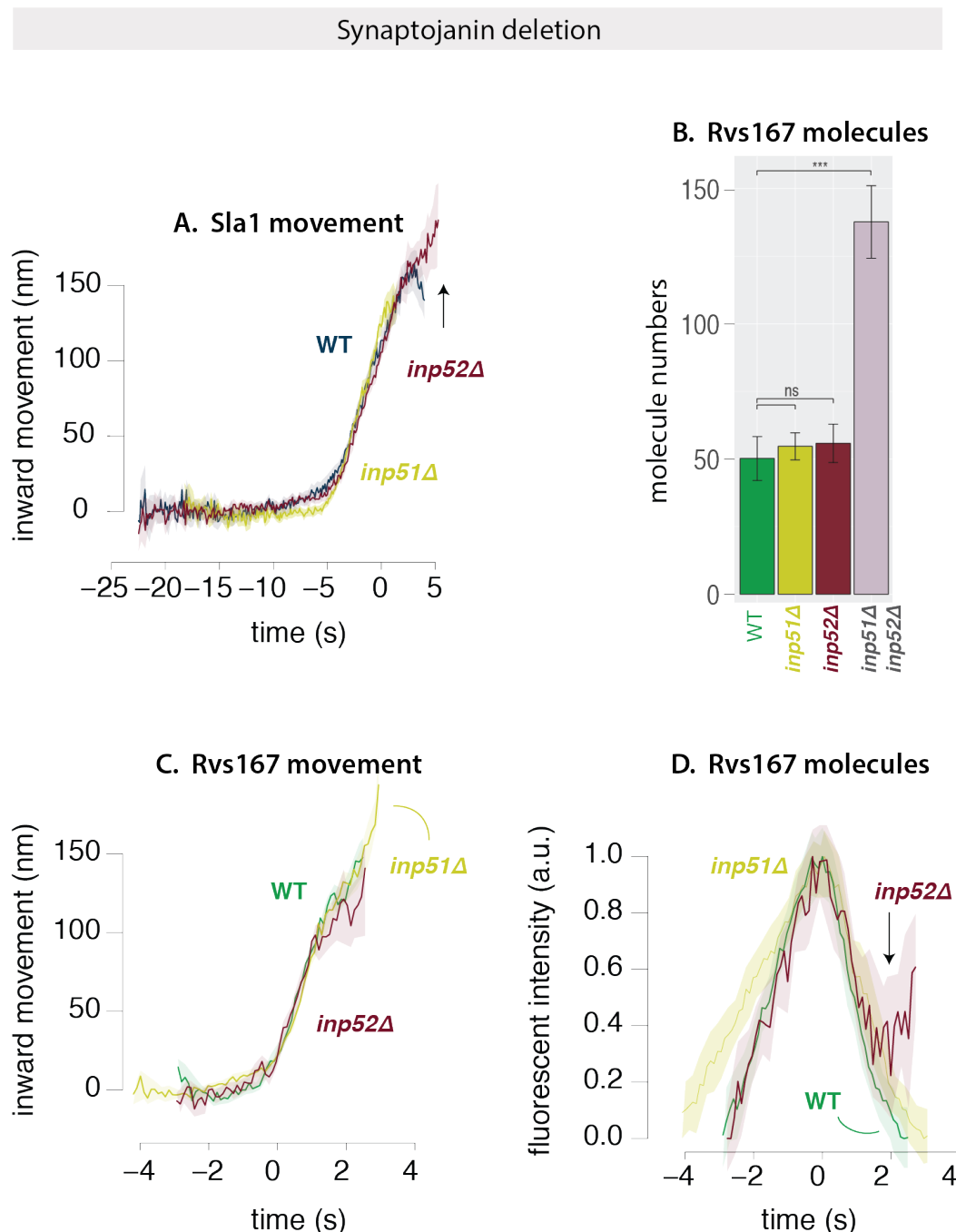


Figure 3.8 – A: Movement of Sla1 in WT, *inp51Δ* and *inp52Δ* cells. Time=0 (s) for WT Sla1 centroid corresponds to scission time. Sla1 centroids for *inp51Δ*, *inp52Δ* are shifted to move inwards at the same time as WT. **B:** Median number of Rvs167 molecules recruited in WT, *inp52Δ*, *inp52Δ* and *inp51Δ**inp52Δ* cells. P-values from two-sided z test, * = $p \leq 0.05$, ** = $p \leq 0.01$, *** = $p \leq 0.001$. **C:** Movement of Rvs167 in WT, *inp51Δ* and *inp52Δ* . **D:** Normalized fluorescent intensity of averaged Rvs167 patches in WT, *inp51Δ* , *inp52Δ* cells.

Analysis of the *inp51Δ inp52Δ* phenotype is compounded by the retention of endocytic proteins on vesicles. If Rvs, coat, and other components are not recycled from vesicles because of *inp52Δ*, I am unable to distinguish between membrane tubes and vesicles that remain in the vicinity of newly forming membrane tubes. Further, this failure to recycle affects recruitment of protein to new endocytic sites and I cannot separate the effect of failure to recruit protein from scission failure. That *inp51Δ inp52Δ* phenotype results in more aberrations in Rvs dynamics, and previously reported morphological defects than single deletions suggest the two proteins function in separate but partially overlapping pathways²⁹. Defects caused by *inp51Δ* are then partially compensated for by *Inp52*, and vice-versa, but deletion of both results in large defects in cellular processes.

Rvs generates frictional forces on the membrane Recent in-vitro experiments have proposed protein friction as a BAR-driven mechanism for membrane scission³³. In this model, a BAR domain scaffold on a membrane tube forms a frictional barrier to lipid diffusion. Forces that pull on the membrane increase the frictional force exerted by the scaffold on the underlying membrane tube. This leads to membrane thinning in the region not covered by the BAR, since there is no lipid influx. In turn, this leads to increased membrane tension in this region. Eventually, membrane pores form in this portion of the tube, which break the tube, forming a vesicle. In-vivo, the forces pulling the membrane could be provided by molecular motors like myosins or actin polymerization. This model predicts that if more BAR proteins are added, and at a faster rate, to the membrane, frictional force would increase. If frictional force increases, scission would occur faster: that is, at shorter invagination lengths compared to a membrane with fewer BAR proteins.

3.4.3 Membrane scission does not occur at shorter tube lengths with more Rvs

To test whether protein friction could effect membrane scission in yeast, I duplicated the Rvs167 and Rvs161 genes as described in Huber et al³⁴. Gene duplication is performed in haploid cells to produce strains that have one (WT in haploids: 1xh) and two copies (2xh) of both Rvs161 and Rvs167 genes. These haploid strains are then mated to generate diploid strains that have four copies of Rvs167 and Rvs161 genes (4xd), two copies (WT in diploids: 2xd). Cells containing 1x copy of Rvs is generated by crossing *rvs167Δstrain* with an *rvs161Δstrain* (1xd). Compared to haploid strains expressing Rvs167-GFP, diploid strains appear to have more endocytic patches (Fig.3.9B).

Sla1 and Rvs in gene duplicated haploids: In Fig.3.9A, Sla1 movement in WT (1xh) and duplicated (2xh) haploids are presented. WT Sla1 is aligned so that time= 0 (s) corresponds to scission time. Sla1 for 2xh is shifted so that it moves inwards at the same time as WT. Both Sla1 centroids move inwards at the same rate, and to the same distance of 140nm.

I measured the number of Rvs molecules recruited to endocytic sites in 1xh and 2xh strains. The maximum number of Rvs molecules recruited in the 2xh strain is 180, compared to 114 in WT (see 3.1, Fig.3.9C): 1.6x more Rvs is recruited to endocytic sites in the gene duplicated strain. In Fig.3.9C, fluorescent intensity of Rvs167 in 1xh and 2xh cells are shown. Both Rvs167 fluorescent intensity plots are aligned so that time=0 (s) corresponds to their respective maxima. Rvs accumulation takes the same amount of time in 1xh as in 2xh: rate at which Rvs molecules is recruited to endocytic sites is 1.6x in Rvs duplicated cells.

Dynamics of Rvs disassembly are quite different. Fig.2.8B shows that disassembly is slowed by 1.5 seconds in 2xh compared to 1xh cell. In the corresponding Rvs centroid movement traces (Fig.3.9C), instead of the sharp jump seen in WT, there is a delay in movement into the cytoplasm.

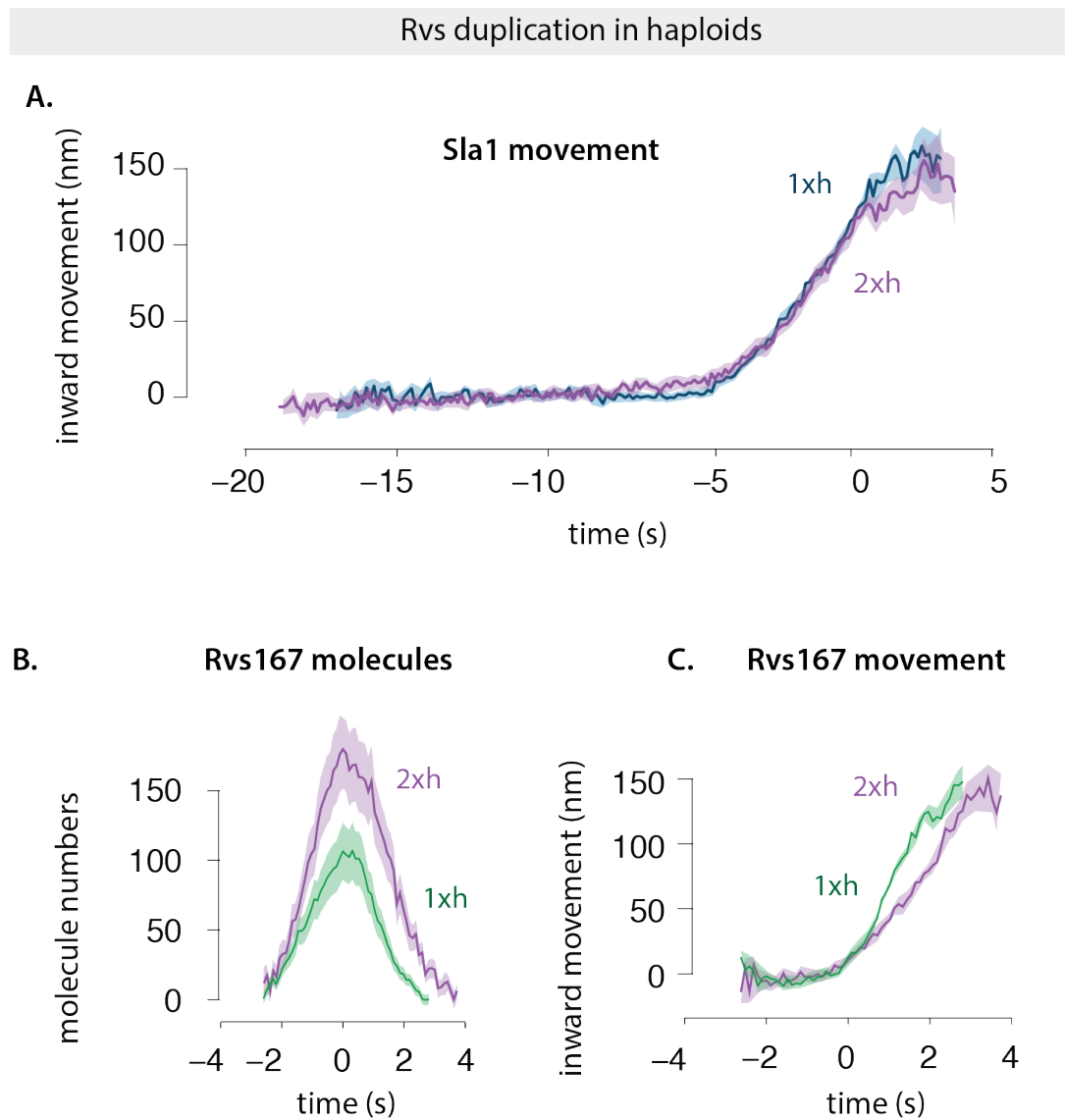


Figure 3.9 – A. Movement Sla1 in haploid cells containing 1 (WT, 1xh) and 2 copies (2xh) of Rvs161, Rvs167 genes. Sla1 centroid in 1xh is aligned so that time=0 (s) corresponds to scission time. Centroid of 2xh Sla1-GFP is shifted to move inwards at the same time. B. C Molecule numbers and movement of Rvs167 to sites in 1xh and 2xh cells. In B and C, 1xh is aligned to scission time. 2xh is shifted to move inwards at the same time as 1xh

Sla1 and Rvs in gene duplicated diploids: In diploid cells expressing 1 (1xd), 2 (2xd), and 4 (4xd) copies of Rvs, Sla1 movement, Rvs dynamics, and recruitment numbers are compared. In Fig.3.10B, Sla1 in the three cell types are shown. In all cases time=0 (s) corresponds to scission time. Sla1 movement is the same in 4xd and 2xd cells: they move at the same rate, and to the same lengths of about 140nm. In 1xd strain, Sla1 movement rate is the same till about 110nm, and

is then slightly reduced. Sla1 movement in 1xd suggests that vesicle scission occurs at invagination lengths about 10nm shorter than that in 2xd and 4xd.

Rvs167 movement and fluorescent intensities are shown in Fig.3.11A, B. Magnitude of inward movement of the Rvs is similar for the 4xd, 2xd and 1xd. In the 1x strain, however, the centroid disappears immediately after scission, suggesting that there is reduced Rvs at the base of the newly formed vesicle compared to the 2xd and 4xd.

Recruitment dynamics of Rvs in all three are different: in the 4xd strain, Rvs is recruited at a rate of about 51 molecules/second, which is reduced to 27.5 molec./sec. for 2xd and 13.6 molec./sec. for the 1xd. Recruitment of Rvs is not directly proportionate to gene copy number: maximum number of Rvs recruited increases from 101 from in the 2x Rvs strain to 143 in the 4x strain (see TABLE1). In the 1x Rvs strain, 80 molecules of Rvs are recruited before scission occurs. In order to determine whether this is a reflection on protein availability or if something else limits recruitment of Rvs, I roughly quantified the cytoplasmic intensity of Rvs167-GFP in the respective strains, and scaled them to 2xd to obtain a ratio of cytoplasmic intensity compared to the WT. The number of molecules recruited to endocytic sites scales with the amount of protein in the cytoplasm (see methods).

Abp1 amounts in gene duplicated diploids: I measured the amount of Abp1 at endocytic sites in 4xd, 2xd, and 1xd diploid cells. Abp1 numbers provided in Fig.2.10B are quantified in cells containing Rvs167-GFP and Abp1-mCherry. Abp1-mCherry signal is then scaled to Nuf2-mCherry, similar to quantification method in Picco et al. that uses GFP instead of mCherry. Fig2.10B shows that even though the number of Rvs molecules recruited varies depending on number of Rvs gene copies, the same amount of Abp1 is recruited to endocytic sites in all three cases. In the Abp1 quantification in this case, only one allele of Abp1 is tagged with mCherry. The total amount of Abp1 is double the numbers reported here.

Rvs gene duplication data suggests that even if Rvs is recruited up to 1.6x faster than in WT cells, membrane invaginations do not change in length. That the same amount of Abp1 is recruited irrespective of amount of Rvs suggests that the system is sensitive to amount of

Abp1 rather than Rvs. Scission time is therefore likely to be triggered by the amount of force generated by the actin network.

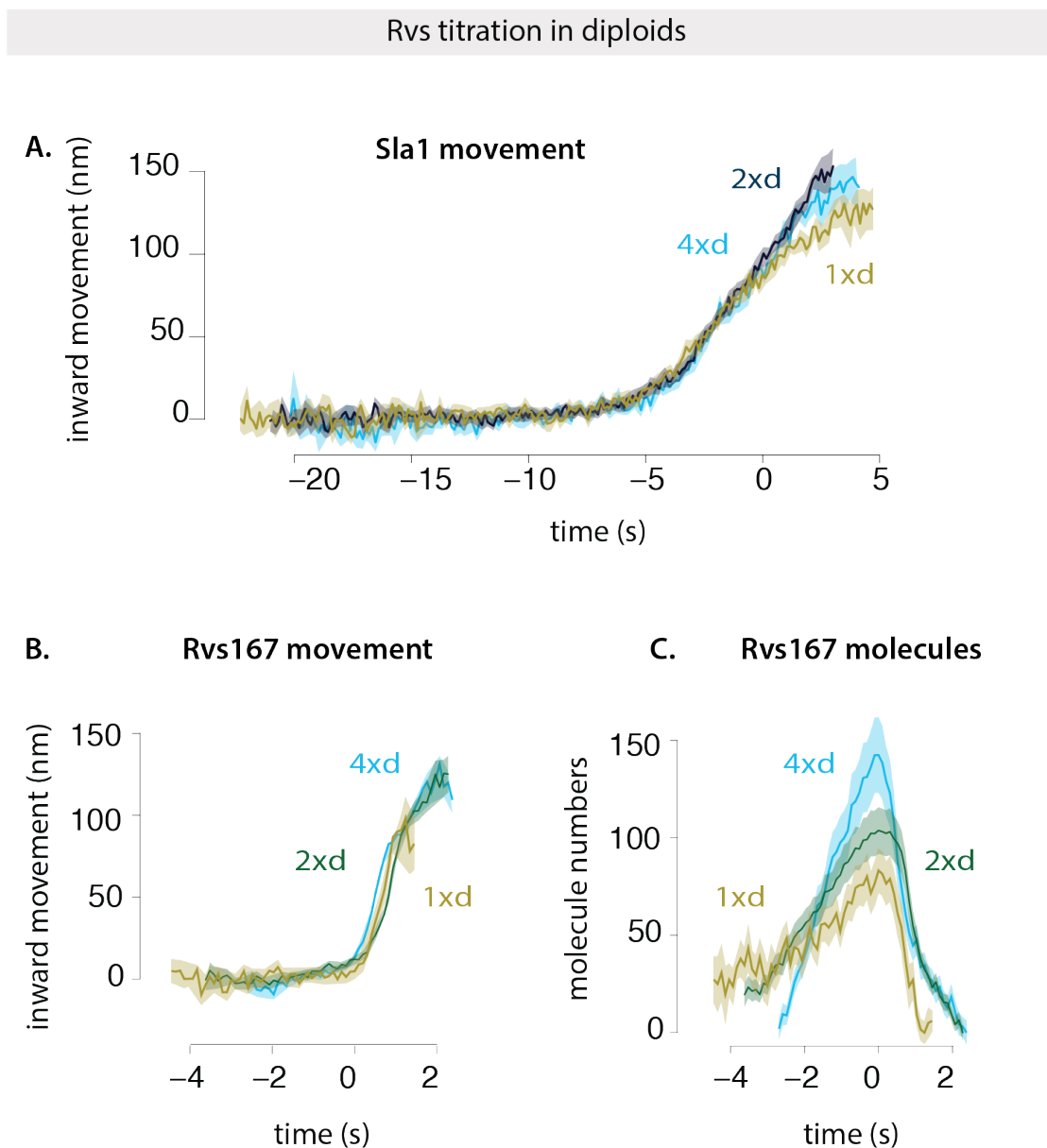


Figure 3.10 – A. Movement of Sla1 in diploid cells containing 1 (2xd), 2 (WT, 2xd) and 4 copies (4xd) of Rvs161, Rvs167 genes. Sla1 centroids for 2xd, 4xd are aligned so that Time=0 (s) corresponds to scission time. 1xd Sla1-GFP centroid is shifted to move inwards at the same time as the other two. B. Rvs167 movement in 1xd, 2xd and 4xd cells. All are aligned so that time=0 (s) corresponds to maximum molecules recruited. C. Number of molecules of Rvs167-GFP in 1xd, 2xd, 4xd cells. Time=0 (s) corresponds to maximum molecules.

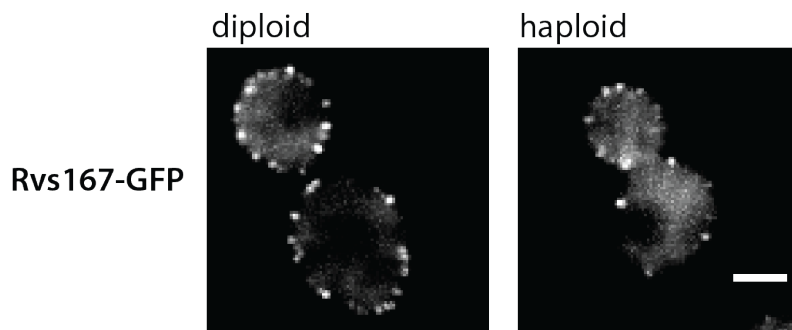
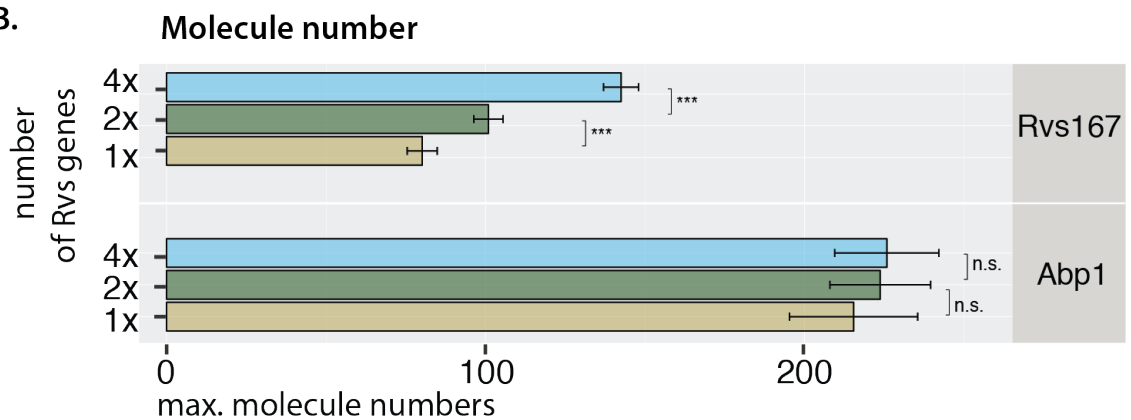
A.**B.**

Figure 3.11 – A. Maximum intensity projection of haploid and diploid cells expressing Rvs167-GFP. Scale bar =2um. B. Maximum molecule number and standard error of mean of Rvs167-GFP and Abp1-mCherry in diploid strains. Only one allele of Abp1 is tagged with m-Cherry, so double the amount shown here is expected to be recruited. P-values from two-sided z test, * = $p \leq 0.05$, ** = $p \leq 0.01$, *** = $p \leq 0.001$.

BAR domains as membrane scaffolds The capacity for BAR domains to oligomerize and tubulate liposomes has proposed membrane scaffolding as a possible function *in vivo*. As membrane scaffolds, they would impose their own curvature on the underlying membrane and stabilize this shape. There are some requirements for a protein complex to act as a scaffold³⁵:

1. it must have a defined membrane interface
2. it must have an intrinsic curvature
3. it must present be rigid in structure, and
4. membrane binding surface must be large enough to induce curvature

BAR domains present a curved shape as membrane interacting surface^{13,36,37}, and have the capacity to oligomerize into large assemblies on tubes^{9,38,39}. It has also been shown that the central BAR region is rigid and required for tubulation, both *in-vivo* and of liposomes⁴⁰. BAR domains therefore meet all of these requirements.

It has been shown that BAR domains can prevent membrane scission by scaffolding the membrane, allowing formation of stable tubular structures and preventing vesiculation of these structures^{5,12}. In simulations, adding BAR domains to an invaginating tube removes membrane shape instabilities. Actin forces, membrane rigidity and tension, and turgor pressure result in a wide invagination tip and shrinking tubular region that result in membrane shape instability and therefore scission. Adding curved BAR domains that have a preferred radius of curvature results in stabilization of the membrane shape and prevents scission³⁴.

3.4.4 Coat movement is influenced by recruitment of BAR domain

As observed in the previous section ??, Sla1 movement is decreased by decreased recruitment of Rvs, although adding excess protein does not influence it. In BAR cells Sla1 movement is reduced from WT to close to that of rvs167 Δ . However, Rvs recruitment is also decreased. Reduced coat movement therefore could result from loss of the SH3 domain, or from reduced Rvs recruitment. To test this,

I duplicated as described before, the BAR domain alone in haploid yeast cells. This results in two copies of the BAR domain (2xBAR). I then compared Sla1 and Rvs in 2xBAR against BAR (1xBAR), WT Rvs (1xh), duplicated Rvs (2xh), and rvs167del.

I compared recruitment of Rvs in the different cells. As shown in Fig.3.12C, 1x BAR is recruited at low copy numbers compared to WT . Maximum molecules recruited is 57 ± 9.9 , about 50% that of WT. Duplication of the BAR domain in 2x BAR increases this recruitment to 90.58 ± 9.6 . Compared to WT, recruitment of BAR domains increases to 62

Sla1 moves inwards at a rate of about 26nm/s. While duplication of the full-length Rvs genes does not change the rate of inward movement of Sla1, total rate of inward movement is reduced to 13.3nm/s in 1x BAR case. This rate increases to about 18nm/s in the 2x BAR case. Adding BAR domain increases the speed of inward movement, as well as depth to which Sla1 moves. Sla1 centroid in rvs167 deleted cells shows a movement similar to 1x BAR case. Rvs167 dynamics similar to WT can also be recapitulated by adding increasing amounts of Rvs167 (Fig.3.12B,C).

This shows that shallow invaginations of the rvs167 Δ can be rescued by recruiting only BAR domains of Rvs167.

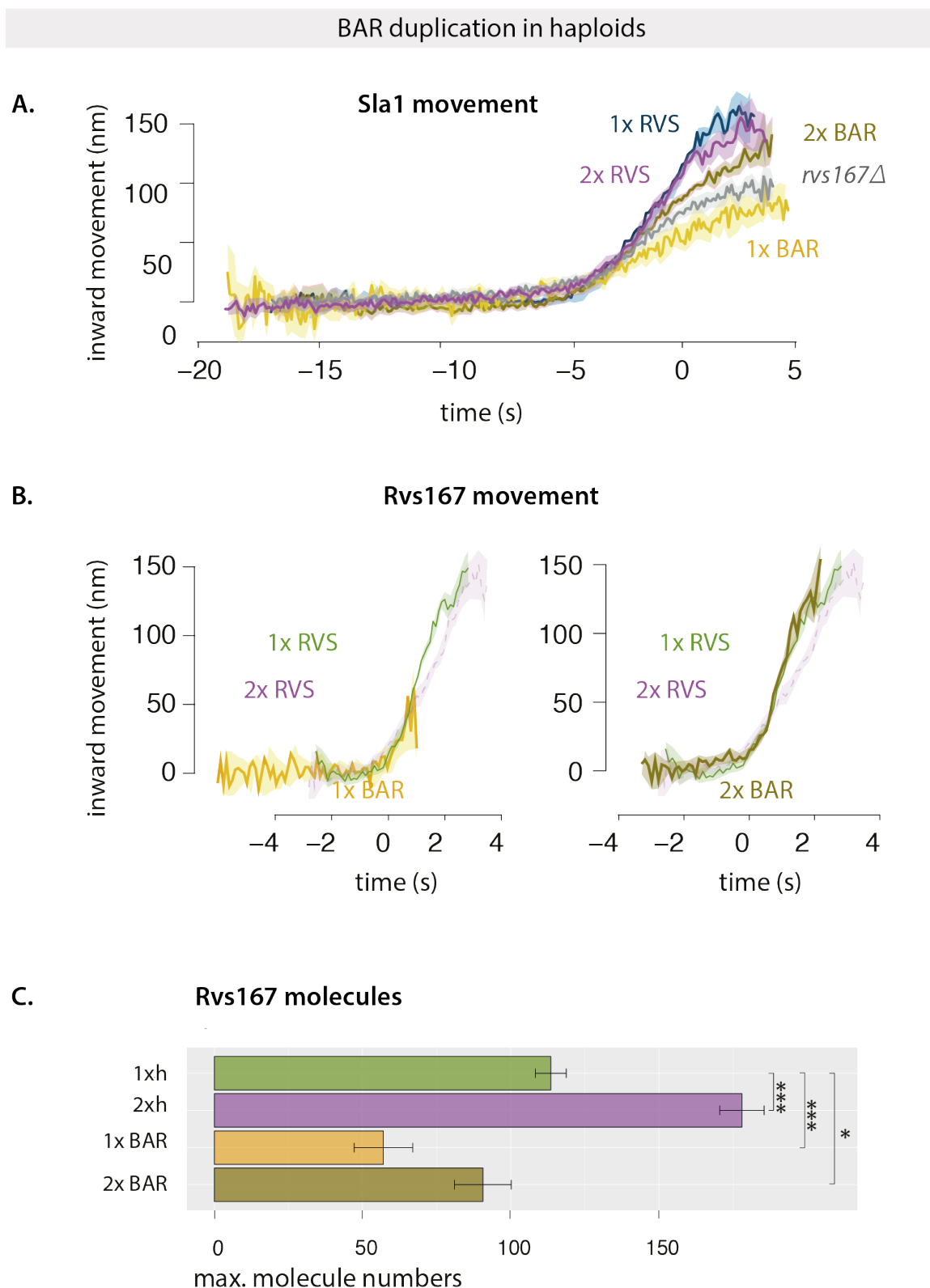


Figure 3.12 – A: Movement of Sla1 in haploid cells consisting of 1 (WT, 1xh) and two copies (2xh) of Rvs genes, 1 (1xBAR) and 2 copies of BAR domain (2xBAR) and *rvs167Δ* cells. Time=0 (s) for WT Sla1 is scission time. Other centroids shifted to move inwards at the same time as WT. **B:** Movement of Rvs167 in 1xh, 2xh, 1xBAR, 2XBAR cells. Time= 0 (s) for WT corresponds to scission time. Other centroids shifted to move inwards at the same time as WT. **C:** Maximum molecule number and standard error of mean of Rvs167-GFP at endocytic sites. P-values from two-sided z test, * = $p \leq 0.05$, ** = $p \leq 0.01$, *** = $p \leq 0.001$.

Rvs as a scaffold against turgor pressure Pressure, membrane tension, and rigidity influence the shape of membrane invaginations. In yeast, a high turgor pressure of 0.6 - 0.8 MPa pushes the plasma membrane against the cell wall. This pressure is opposed by the rigid cell wall, and the endocytic machinery must exert forces to bend and pull the plasma membrane away from the cell wall into the cytoplasm. Forces from actin polymerization are hence necessary to overcome this resistance to membrane invagination. In serge et al., simulations show that membrane tension has a negligible influence on forces required to pull the membrane. Shape of the membrane is dominated by membrane rigidity and turgor pressure. Membrane rigidity, which comes from the properties of the lipids and proteins embedded in it shapes the shape of the top of the invagination that is pulled up. Turgor pressure pushes inwards the membrane neck, constricting it.

Turgor pressure can be controlled by osmoregulating agents like sorbitol. Sorbitol treatment causes cells to expel water and increase the internal concentration of osmolytes to match that of the environment. When the cell expels water, they shrink in size, resulting in a brief decrease of turgor pressure. Loss of turgor pressure is compensated by Gpd1, which increases glycerol production in cells, and increases turgor pressure within 10 minutes of sorbitol treatment.

In fission yeast *S.pombe*, treatment with sorbitol shortens the time between arrival of the coat protein Sla1 and actin-binding protein App1, but does not affect the inward movement of the coat⁴². Sorbitol rescues the invagination defect of partially blocking actin with low doses of LatA. At 0.2M sorbitol, 90% of Sla1 patches in these cells move inwards for 50nm instead of 300nm, but retract back to the plasma membrane.

Some WASP/Myosin mutations can be rescued by reducing turgor pressure. Deletion of myosin results in failure to invaginate, and this can be rescued up to 70% when treated with 0.2 M Sorbitol. Loss of Fimbrin, which bundles actin filaments, and is also necessary for membrane invagination, can also be rescued by sorbitol. These experiments show that some defects in the force generation system can be compensated by lowering turgor pressure. Since sorbitol decreases the amount of time between App1 arrival and movement, reducing turgor pressure likely lowers the threshold force required to pull

the membrane in the early stages of invagination. Consistent with this, simulations of Serge et al., show that the force requirement for membrane invagination is highest in the beginning of the invagination process.

An extension of the scaffold hypothesis for Rvs is that it protects the membrane tube against the high turgor pressure inside yeast cells. Reducing turgor pressure could then remove the requirement for Rvs scaffolding.

3.4.5 Requirement for Rvs is unchanged by membrane tension

In order to test if the role of the Rvs scaffold is to counter the membrane constricting effect of turgor pressure, I studied Sla1 and Rvs in WT and rvs167 Δ cells treated with 0.2M sorbitol. At higher concentrations of sorbitol, cells shrivel and do not recover from turgor pressure loss⁴².

In Fig.3.13, Sla1 movement in WT and rvs167 Δ cells with and without sorbitol is shown. WT Sla1 is aligned so that time=0 (s) corresponds to scission time. The other three centroid movements are shifted so that they move inwards at the same time as the WT. WT cells treated with sorbitol do not show any change in inward movement of Sla1. Both centroids move to the same lengths of 140nm at the same rate, consistent with *S.pombe* data from Basu et al. In rvs167 Δ cells, Sla1 moves to about 80nm. In rvs167 Δ cells treated with sorbitol, there is no difference in the movement. Both Sla1 centroids move at the same rate, and to the similar invagination lengths.

This shows that the Rvs scaffold does not serve to counter turgor pressure.

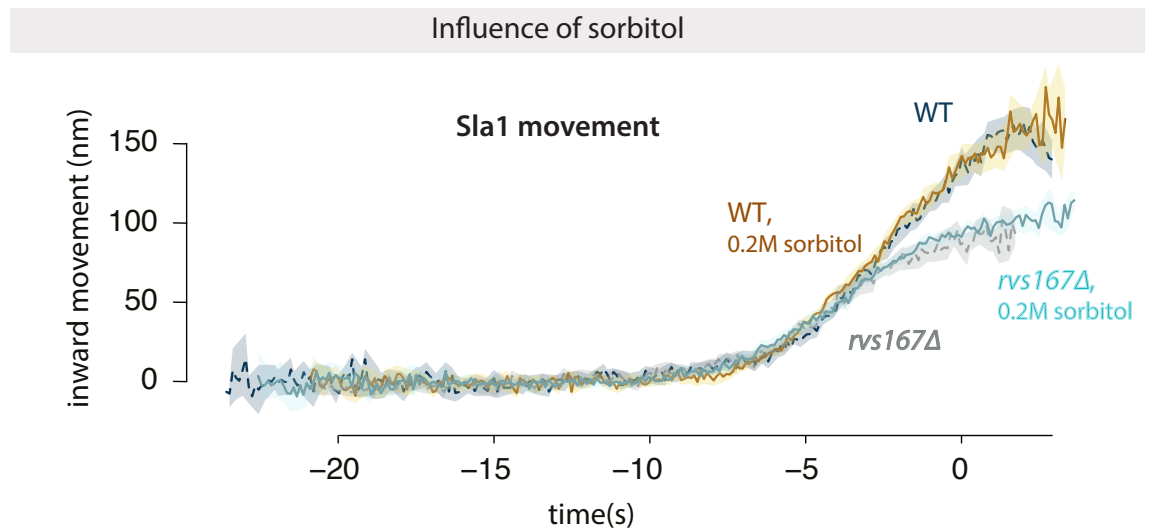


Figure 3.13 – Movement of Sla1-GFP in WT, WT cells treated with 0.2M sorbitol, *rvs167* Δ and *rvs167* Δ cells treated with 0.2M sorbitol. WT Sla1-GFP aligned to scission time, other centroids moved to move inwards at the same time as WT.

PLOIDY	PROTEIN	GENOTYPE	MEDIAN NUMBER	S.E.M
Haploid	Abp1	WT	253.1	19.9
	Abp1-mCh	WT	347	30.6
	Abp1	BAR	172.6	12.9
	Abp1-mCh	Rvs167, Rvs161 2x	260.7	21.3
	Rvs167	WT	53.2	5.2
	Rvs167	BAR	30.1	9.9
	Rvs167	51del	54.7	5
	Rvs167	52del	55.8	7.1
	Rvs167	51del52del	137.7	13.4
	Rvs167	Bzzdel	49.2	4.8
	Rvs167	Rvs167 2x	57.3	7.5
	Rvs167	Rvs167, Rvs161 2x	82.7	7.5
	Rvs167	BAR 2x	43.6	9.6
	Rvs167	BAR, Rvs161 2x	41.3	8.4
Diploid	Abp1-mCh	WT (2x Rvs)	131.4	15.8
	Abp1-mCh	4x Rvs	124.1	16.3
	Abp1-mCh	1x Rvs	126.5	20.1
	Rvs167	WT (2x Rvs)	55.9	4.6
	Rvs167	4x Rvs	63.7	5.5
	Rvs167	1x Rvs	44.8	4.7
	Rvs167	Rvs mismatch	31.1	8.6

Table 3.1 – *= Number of molecules was quantified in cells containing one tagged allele of Abp1-mCherry.

4 | Discussion

Recruitment and function of the Rvs complex in has been explored in this work, as well as several models for how membrane scission could be effected in yeast endocytosis. I propose that Rvs localizes by interactions of the BAR domains of the Rvs complex with invaginated membranes, and that the SH3 domain is required for efficient recruitment of Rvs to sites. Arrival of Rvs on membrane tubes scaffolds the membrane tube and prevents membrane scission, in a manner that depends on recruitment of a critical number of Rvs molecules, till actin forces rupture the membrane, causing vesicle scission, and releasing Rvs molecules. Here I discuss the main findings of this thesis in support of these propositions.

4.1 Recruitment of Rvs to endocytic sites

Rvs is relatively short-lived protein at endocytic sites, recruited only once membrane tubes once they are formed (Picco et al. 2015; Kukulski et al. 2012; Kaksonen, Toret, and Drubin 2005). FCS measurements have shown that the cytoplasmic content of Rvs167 and Rvs161 is quite high compared to other endocytic proteins (Boeke et al. 2014). Many endocytic proteins like Las17, Vrp1, type1 myosins, are measured at 80-240nM, while cytoplasmic intensity of Rvs161 and 167 is 721nM and 354nM respectively. In spite of this, relatively few numbers of Rvs are recruited to endocytic sites, suggesting that cytoplasmic concentration alone may not determine recruitment. Comparison between FCS measurements of cytoplasmic concentration for different endocytic proteins, and their recruitment to the endocytic sites indicates low correlation between the two, perhaps unsurprisingly, requiring that other directed mechanisms recruit proteins in

a timed and efficient manner. In the case of Rvs, both timing and efficiency appear crucial to its function, the question is what confers both.

4.1.1 The BAR domain senses membrane curvature

The curved structure of the BAR dimer has suggested that Rvs is recruited by its preference for some membrane shapes over others, supported by its arrival at curved membrane tubes. In the absence of membrane curvature, in *sla2Δ* cells, the BAR domain alone does not localize to cortical patches (Fig.3.3D). This demonstrates for the first time that the BAR domain does indeed sense and requires membrane curvature to localize to cortical patches. Work on BAR domains have proposed that electrostatic interactions between positive charges at the concave surface and tips of the BAR domain structure and negatively charged lipids mediate membrane binding. Mutations in these lipid-binding surfaces would clarify the interaction with underlying lipids, and test if Rvs relies on similar interactions.

4.1.2 BAR domain times recruitment of Rvs

In BAR cells, Rvs167 is able to localize to endocytic sites, and has a similar lifetime in WT cells (Fig.3.3, Fig.3.4). In Fig.3.4 B,D we see that while in WT, Rvs167 arrives about 4 seconds after the arrival of Abp1, in BAR cells it arrives only 6 seconds after Abp1 arrives. There is a time delay between Abp1 and Rvs167 recruitment in BAR cells, confirmed by the TIRF measurement in 3.4D.

The delay in recruitment could occur because the membrane has not acquired the required invagination lengths or because the loss of the SH3 domain has delayed recruitment. That the delay comes from the absence of a particular invagination length is supported by the fact that Sla1 moves inwards at a slower rate in BAR cells. It takes longer for the membrane in BAR cells to reach the same length as WT. Rvs167 arrives in BAR cells when Sla1 has moved inwards 25-30nm (dashed red lines in Fig.3.4A), which is also the distance Sla1 has moved when Rvs167 arrives in WT. To be noted is that Sla1 is not

directly at the plasma membrane, and the centroid of Sla1 sits about 20nm higher on the plasma membrane than Sla2(Picco et al. 2015). Therefore, a 25-30nm distance of Sla1 would correspond to 45-50nm of membrane invagination, by which point the membrane is already tubular (Picco et al. 2015; Kukulski et al. 2012), consistent with Rvs arrival at invaginated tubes. This suggests Rvs recruitment is timed to specific membrane invagination length, and that this timing is provided by the BAR domain.

4.1.3 The SH3 domain makes Rvs recruitment efficient

As seen in Fig.3.4C, Rvs167 in BAR cells accumulates to about half the WT number, even though the same cytoplasmic concentration is measured (see methods). This indicates that the SH3 domain increases the efficiency of recruitment of Rvs. Either SH3 domains help recruitment to endocytic sites, or it stabilizes interaction with sites. It is also possible that SH3 domains stabilize dimers of the Rvs complex. Since the cytoplasmic signal of Rvs167 is the same in both WT and BAR cells, and Rvs167 and Rvs161 have been shown to exist as dimers in the cytoplasm (Boeke et al. 2014), it is unlikely that loss of the SH3 domain destabilizes the Rvs complex. In *sla2Δ* cells, full-length Rvs can assemble on the membrane (Fig.3.3D-F). Since there is no BAR-membrane interaction in *sla2Δ* cells, this supports a role for the SH3 domain in increasing recruitment of Rvs by clustering protein molecules.

4.1.4 The SH3 domain can assemble and disassemble Rvs molecules independent of the BAR domain and actin interactions

As mentioned above, in *sla2Δ* cells, full-length Rvs is able to localize to cortical patches without the curvature-dependent interaction of the BAR domain (Fig3.3D-F). The independent ability of the SH3 domain to localize and disassemble protein is unexpected. This indicates that the SH3 domain is able to mediate recruitment of an Rvs patch, and then disassemble this patch.

In *sla2Δ* cells treated with LatA (Fig.3.3G-H), actin-based membrane curvature, as well as actin-binding proteins are removed from the plasma membrane. Full-length Rvs167 in these cells show transient localizations at the plasma membrane (Fig.2A). In BAR + *sla2Δ* cells with LatA treatment, this localization is lost, suggesting that the former is dependent on SH3 domain interaction, and that this is independent of both actin and membrane curvature.

Abp1 is an activator of the Arp2/3 complex

4.1.5 SH3 domain times affects actin dynamics

In WT cells, the Abp1 and Rvs167 fluorescent intensity reach maxima concomitantly, and the consequent decay of both also coincide. That this occurs at the same time indicates that upon vesicle scission, the actin network is immediately disassembled. Membrane scission essentially occurs around the intensity peak of the two proteins. This coincident peak is lost in BAR cells. Rvs in these cells peaks several seconds after Abp1 intensity starts to drop, and the decay of Abp1 is prolonged, taking nearly double the time as in WT. As we see in Fig.3.4C, the number of Abp1 molecules recruited is decreased to about two thirds the WT number. Although it is not clear what the decoupling of Abp1 and Rvs peaks mean, the changes in Abp1 dynamics suggests a strong disruption of the actin network. SH3 domains are known to interact with components of the actin network, but study of other components of the actin machinery is required to understand how exactly loss of the SH3 has changed the progression of endocytosis.

4.1.6 What does the SH3 domain interact with?

SH3 interaction with an endocytic binding partner could help recruit Rvs to sites. Many such interaction partners have been proposed. Abp1 interaction with the Rvs167 SH3 domain has been shown (Lila and Drubin 1997; Colwill et al. 1999), as has one with WASP protein Las17 (Liu et al. 2009; Madania et al. 1999), yeast Calmodulin Cmd1 (Myers et al. 2016), type I myosins (Geli et al. 2000), and Vrp1 (Lila and Drubin 1997). These proteins are currently being studied

as potential targets of the Rvs167 SH3 domain. All of these suggested binding partners localize to the base of the invagination (Yidi Sun 2006; Picco et al. 2015), and do not follow the membrane into the cytoplasm. If one of these is the SH3 interaction partner, SH3 domains interact with the endocytic network at the base of the invagination. Centroid tracking however, suggests that Rvs is accumulated all over the membrane tube without bias towards the base of the invagination. If Rvs was recruited to the base and pulled up as the invagination grows, the centroid would move continuously upwards rather than remain relatively non-motile before the jump at scission time. It is possible that the SH3 initially helps cluster near the base, and as the membrane invaginations grow longer, BAR-membrane interactions dominate.

It is unclear how Rvs is arranged on the membrane tube. Although solved structures of BAR domains show high structural similarity in spite of low sequence similarity, no structure for the Rvs complex exists. The fact that this is a hetero- rather than homodimer suggests that the structure does not necessarily resemble that of Amphiphysin or Endophilin homodimers, and a high-resolution structure will be necessary to clarify the interaction and arrangement of Rvs on endocytic tubes

4.1.7 Total number of Rvs recruited is independent of ploidy

When ploidy is doubled from haploids to diploids, we could expect that double the protein amount is expressed and recruited, but it does not appear so. The amount of Rvs recruited in WT haploid (1xh) and diploids (2xd) remain about the same, and cytoplasmic signal is similar (Fig.4.1). This is not a very robust estimate for cellular expression, and needs to be verified by quantitative western blots. However, the invariance between accumulated protein in haploids and diploids shows that Rvs recruitment is not determined by the number of alleles of Rvs. Haploid and diploid cells appear to tune the amount of Rvs recruitment to get a specific amount to endocytic sites.

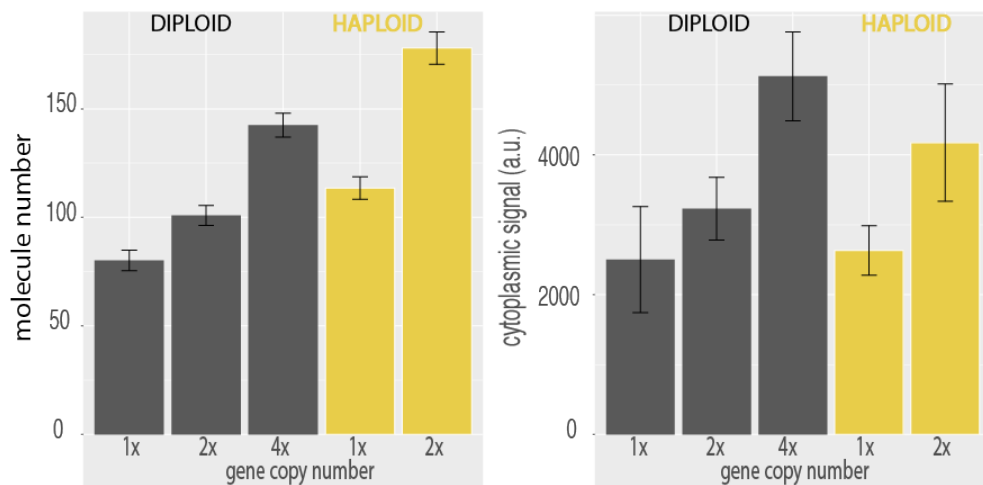


Figure 4.1 – A. Maximum molecule number of Rvs167-GFP recruited with S.E.M in haploid and diploid cells with different gene copies of Rvs. B. Cytoplasmonic signal of Rvs167-GFP with standard deviation in haploid and diploid cells with different gene copies of Rvs.

4.1.8 Rvs recruitment rate increases with increasing gene copies

In diploids, the genome that contains four copies of Rvs (4xd) could be expected to express and recruit twice the amount of Rvs as one that contains two copies (2xd). However, cytoplasmonic signal increases by 1.6x and recruitment to endocytic sites increases only by 1.4x. Doubling the gene copies appears not to double protein expression or recruitment in the case of Rvs. Similarly, duplicating Rvs genes in haploids results in an increase in number of molecules recruited, but not in doubling (1xh, 2xh). Although the rate of adding Rvs is different in haploids and diploids, in both cases, it increases by gene copy number.

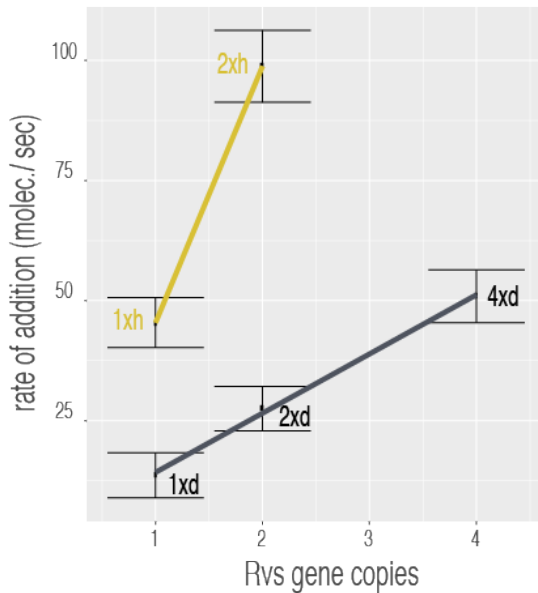


Figure 4.2 – Rate of Rvs molecules added to endocytic sites before scission vs gene copy number in haploids and diploids. SEM of the molecule numbers recruited, and linear fit through the data is shown.

The rate of Rvs recruitment is slower in WT diploid compared to WT haploid (2xd vs 1xh, Fig.4.2). Diploid cells do not double in volume compared to haploids: under normal growth conditions, the volume of the diploid cell is around 1.57x that of the haploid cell, and the average cell surface area increases to about 1.4x (Weiss, Kukora, and Adams 1975). It is possible that the delay in recruitment is arises from the fact that protein expression remains the same in both. There is a larger surface area and volume, and more endocytic events in diploids. Recruitment could be delayed in diploids because Rvs is recruited from similarly concentrated cytoplasmic pool to more sites, decreasing the local concentration.

Cytoplasmic protein concentration is increased when gene copies are increased, and recruitment to endocytic sites is increased by the increase in cytoplasmic concentration. Although this data needs to be confirmed by quantitative western blots for protein expression, it suggests that how much Rvs is recruited scales with available concentration of protein.

4.2 Arrangement of Rvs

No solved structure for the Rvs complex exists. That Rvs is a hetero-rather than homodimer suggests that the structure need not resemble that of Amphiphysin or Endophilin homodimers, and a high-resolution detail will be necessary to clarify the interaction and arrangement of Rvs on endocytic tubes. It is therefore unclear how Rvs is arranged, although there are some indications from the experiments in this work of the interaction with the membrane.

4.2.1 Rvs does not form a tight scaffold on membrane tubes

In-vitro helices of BAR domains have suggested that Rvs might form a similar helical scaffold. Correlating CLEM and centroid movements has proposed that an Rvs scaffold covers the entire membrane tube up to the base of the future vesicle (Picco et al. 2015).

In diploid Rvs strains, more Rvs can be recruited, at a much faster rate than in WT cells (Fig.3.9 B-C, Fig.4.2). Disassembly dynamics of 4xd, however, is the same as in 2xd (Fig.3.9C, Fig.4.3). The sharp decay of fluorescent intensity of WT Rvs (1xh in haploids, 2xd in diploids) indicates that all of the protein is suddenly released, consistent with a BAR scaffold that breaks upon vesicle scission, releasing all the membrane-bound protein at once. A similar decay in the 4xd strain suggests that all the Rvs here is also bound to the membrane. Since the membrane is able to accommodate 1.4x the amount of BAR protein as the WT, it would suggest that at lower protein amounts, a tight helix that covers the entire tube is not likely. Adding molecules to such a tube would result in a change in Rvs assembly and disassembly dynamics. Further, additional molecules would have to be added at the top or base of a tight scaffold. At the top, the radius of curvature is decreased compared to the tube since this is the rounded vesicle region. At the base, the plasma membrane is flat, and the Rvs BAR domain is similarly unlikely to favour interactions here. Otherwise the scaffold would have to be disrupted to add new molecules, which would likely slow down recruitment rate rather than speed it up.

Molecules could also be added concentric to a pre-existing scaffold. The concave surface of Rvs is known thus far to interact with lipids, and multiple layers of BAR domains on the membrane tube would probably not show the sudden disassembly seen here.

That the membrane surface area does not change in the 4xd compared to 2xd is assumed from the identical movement of Sla1 in both cases (Fig.3.9A). It is possible that a wider tube is formed, which would increase the membrane surface area for BAR binding. This would, however, require the BAR domains to interact with a lower radius of curvature than in WT. This seems unlikely, and in the absence of any indication otherwise, I assume that the membrane tubes in all diploid and haploid cases have the same width.

4.2.2 A limit for how much Rvs can be recruited to the membrane

In the case of Rvs duplication in haploids (2xh), a change in disassembly dynamics is seen (Fig.3.8B, Fig.4.3). In 2xh, the maximum number of molecules recruited is 178 +/- 7.5 compared to WT (1x RVSh) 113.505 +/- 5.2. Nearly 1.6x the WT amount of protein is recruited to membrane tubes. The Rvs167 centroid in 2xh shows a delay in disassembly, suggesting that the excess protein is not directly on the membrane. The excess Rvs either interacts with the actin network via the SH3 domain, or interacts with other Rvs dimers. By a similar argument as 4.2.1 above, I do not expect that multiple layers of BAR domains are formed, and that the excess protein is recruited by the interaction of the SH3 domain.

Whatever the arrangement of the Rvs complex on the membrane, disassembly dynamics is changed in the case of 2xh, compared to all the other haploid and diploid strains. Since the number of Rvs molecules is highest in this strain, this suggests that there is a limit to how much Rvs can assemble on the tube without altering interaction with the endocytic network.

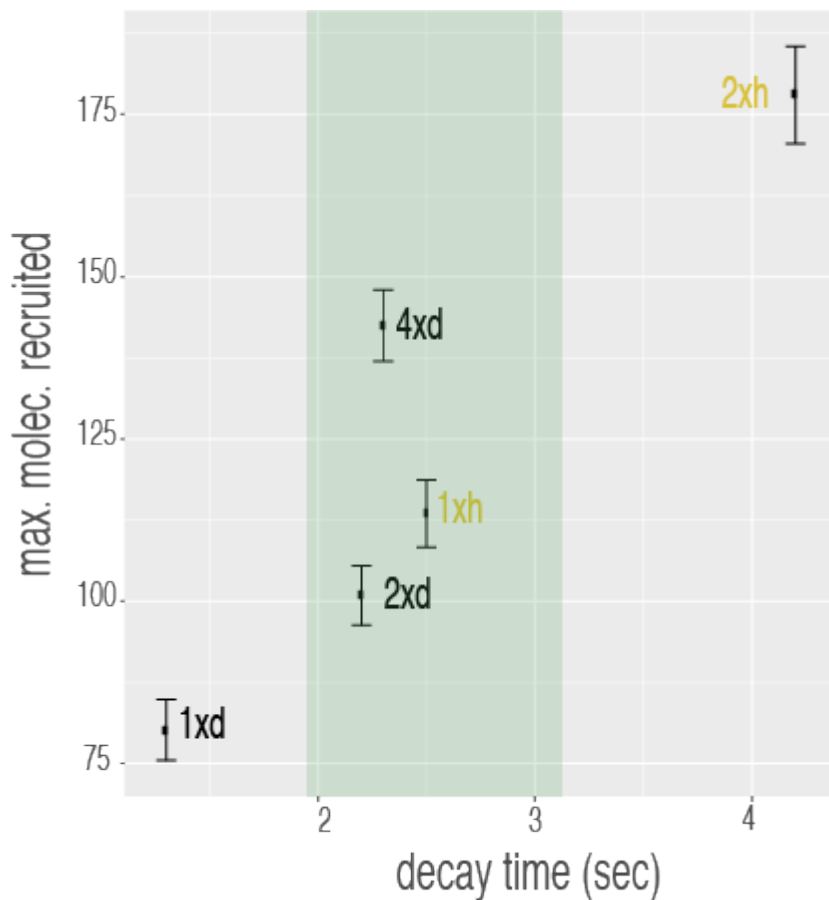


Figure 4.3 – Time from peak of Rvs fluorescent intensity to minimum intensity, against maximum molecule numbers recruited. Coloured region highlights similar disassembly time for increasing amounts of molecules recruited.

Conclusions for Rvs localization All of this data supports that Rvs recruitment rate and total numbers is determined by concentration of protein in the cell. The maximum number of molecules can interact with the membrane is limited by the membrane surface area of the invagination tube. Although more can be recruited, Rvs over a certain threshold interacts in a different way with endocytic sites, likely via the SH3 domain. Timing of recruitment to sites is by curvature-recognition via the BAR domain, while efficiency of recruitment and actin interaction is established via the SH3 domain.

4.3 What causes membrane scission?

4.3.1 Dynamin does not drive scission

Some studies have suggested that dynamin-like Vps1 localizes to endocytic sites, and affects the scission mechanism: Nannapaneni et al(Nannapaneni et al. 2010),, find that the lifetimes of Las17, Sla1, Abp1 increase in the absence of Vps1. Rooij et al (Rooij et al. 2010),, find that Rvs167 lifetimes increase, and are recruited in fewer patches to the cell cortex. On the other hand, *vps1Δ* did not increase the scission failure rate of *rvs167Δ* in other studies (Kishimoto et al. 2011), and did not co-localize with endocytic proteins (Goud Gadila et al. 2017). If Vps1 was to affect scission, the number of failed scission events should increase in *vps1Δ* cells, but I do not find so, confirming other studies (Kishimoto et al. 2011). Vp1 tagged with super-folded GFP and imaged in TIRF does not form cortical patches that co-localize with Abp1-mCherry (data from Andrea Picco, not shown). GFP-tagging could affect the recruitment of Vps1 to endocytic sites while maintaining its role in other cellular processes like vesicular trafficking. Membrane movement and scission dynamics are however, unchanged in the absence of Vps1. If loss of Vps1 prevented or delayed scission, the membrane would continue to invaginate longer than WT lengths, and Sla1 movements of over 140nm would be measured. Rvs centroid movement would likely also be affected: a bigger jump inwards could indicate that that a longer membrane has been cut. That there are no changes in the behaviour of coat and scission markers indicates that if Vps1 is recruited to sites, it is not necessary for Rvs localization or function, and is not necessary for scission.

4.3.2 Lipid hydrolysis is not the primary cause of membrane scission

The synaptojanin-mediated scission model predicts that forces generated by a lipid phase- boundary causes scission (Liu et al. 2006). Synaptojanin-like Inp51 is not seen to localize to the cellular cortex, but cytoplasmic concentration measured by FCS is low (Boeke et

al. 2014), suggesting low levels of expression that are likely not detected by our imaging method. Inp52 localizes to the top of invaginations right before scission, consistent with a role in vesicle formation (Fig.3.6). Predictions of the lipid model do not, however, match our observations.

First, vesicle scission is expected to occur at the interphase of the hydrolyzed and non-hydrolyzed lipid. Since the BAR scaffold covers the membrane tube, this interphase would be at the top of the area covered by Rvs. Kukulski et al. (Kukulski et al. 2012) have shown that vesicles undergo scission at 1/3 the invagination length from the base: that is, vesicles generated by the lipid boundary would be smaller than have been measured. Second, removing forces generated by lipid hydrolysis by deleting synaptojanins should increase invagination lengths, since scission would be delayed or fail without those forces. Deletion of Inp51 and Inp52 does not change the invagination lengths: Sla1 movement does not increase. That the position of the vesicle formed is also unchanged compared to WT is indicated by the magnitude of the jump into the cytoplasm of the Rvs centroid.

There are some changes in the synaptojanin deletion strains. In *inp51Δ* cells, Rvs assembly is slightly slower than that in WT: Inp51 could play a role in Rvs recruitment. In the *inp52Δ* strain, about 12% of Sla1-GFP tracks do not undergo scission. Although this is low compared to the failed scission rate of *rvs167Δ* cells (close to 30%), this data could suggest a moderate influence of Inp52 on scission. Rvs and Sla1 centroids persist after scission *inp52Δ* cells, indicating that disassembly of Rvs on the base of the newly formed vesicle is delayed.

In *inp51Δinp52Δ* cells, Rvs is accumulated at patches, but majority of Rvs patches do not show the typical sharp jump into the cytoplasm. Membrane morphology is hugely aberrant in these cells, complicating interpretation of this data (Srinivasan et al. 1997). Electron microscopy shows long, undulating membrane invaginations, with multiple endocytic sites that are assembled and disassembled, but

fail to undergo scission (Sun et al. 2007; Srinivasan et al. 1997). Where on these long membranes Rvs localizes could be clarified by CLEM or super-resolution microscopy. Large clusters of Rvs seen in the $\text{inp}51\Delta\text{inp}52\Delta$ strain could be multiple Rvs patches on same membrane tube. Pooling signal from multiple endocytic sites would influence the molecule numbers acquired by our analysis, and yield a higher number than at a single site. Rvs does, interestingly, assemble and disassemble. If no vesicles are formed at these membranes, it could indicate that Rvs disassembly is not caused by membrane scission.

4.3.3 Protein friction does not drive membrane scission

Protein-friction mediated membrane scission proposes that BAR domains induce a frictional force on the membrane, causing scission. In Rvs duplicated haploid strains (1xh, 2xh), adding upto 1.6x the WT amount of Rvs to membrane tubes does not affect the length at which the membrane undergoes scission (Fig.3.8). The model introduced in Section 3.4.3 predicts that if more BAR domains were added to the membrane tube, frictional force generated as the membrane is pulled under it will increase, and the membrane would rupture faster. That is, membrane scission occurs as soon as WT forces are generated on the tube. Since BAR domains are added at a faster rate in the 2xh cells, these forces would be reached at shorter invagination lengths. In 2xh cells, WT amount of Rvs is recruited at nearly about -1.8 seconds, but scission does not occur at this time. Instead, Rvs continues to accumulate, and the invagination continues to grow. In diploid strains, adding 1.4x the WT amount of Rvs in the 4x Rvs case also does not change length of membrane that undergoes scission. Protein friction does not appear to contribute significantly to membrane scission.

4.3.4 Actin polymerization generates forces required for membrane scission

Maximum amount of Abp1 measured in all the diploid strains is about 220 molecules (Fig.3.9D). In this case, only one allele of

Abp1 is fluorescently tagged, so half the amount of Abp1 recruited is measured. The maximum amount of Abp1 recruited is then double that measured, which is about 440 ± 20 molecules (assuming equal recruitment of tagged and untagged Abp1). In WT haploid cells, the maximum number of Abp1 measured is 460 molecules, ± 20 molecules. That the same number of molecules of Abp1 is recruited in all cases before scission indicates a dependence on the amount of Abp1, and hence, on the amount of actin recruited. This data is consistent with actin supplying the forces necessary for membrane scission. The membrane ingress continues until the “right” amount of actin is recruited. At this amount of actin, enough forces are generated to rupture the membrane. The amount of force necessary is thought determined by the physical properties of the membrane like membrane rigidity, tension, and proteins accumulated on the membrane (Dmitrieff and Nédélec 2015). Vesicle scission releases membrane-bound Rvs, and coupling of SH3 domains into the actin network could trigger disassembly of the actin network. In the BAR strains, a low amount of actin is recruited (Fig.3.4C). It is clear that in the absence of the SH3 domain, the actin network is severely perturbed, and the effect of this on scission dynamics is currently unclear.

4.4 Function of the Rvs complex

4.4.1 Rvs scaffolds membrane pore

Sla1 in *rvs167 Δ* cells undergoes scission at short invagination lengths of about 60nm (Fig.3.2), compared to the WT lengths of 140nm. This shows that first, enough forces are generated at 60nm to cause scission. Then, that Rvs167 is required at membrane tubes to prevent premature scission. Rvs preventing membrane scission could be explained by the SH3 domain mediating actin forces to the invagination neck: one can imagine that the SH3 domain somehow decouples actin forces from the neck, and this delays scission. Prevention of scission at short invagination lengths can also be explained by Rvs stabilizing the membrane invagination via membrane interactions of the BAR domain (Dmitrieff and Nédélec 2015; Boucrot et al. 2012). Since

invagination depths of *rvs167Δ* cells are increased towards WT lengths by overexpression of the BAR domain alone (Fig.3.10A), I propose that localization of Rvs BAR domains to the membrane tube stabilizes the membrane. This allows deep invaginations to grow until actin polymerization produces enough forces to overcome this stabilization and sever the membrane. Stabilization of the membrane tube increases with increasing amounts of BAR domains recruited to the membrane tube (Fig.3.10). The requirement for Rvs scaffolding cannot be removed by reducing turgor pressure (Fig.3.11), suggesting that the function of the scaffold is not to counter turgor pressure.

4.4.2 A critical amount of Rvs is required to stabilize the membrane

Scission efficiency decreases with decreased amounts of Rvs: in diploids, lowering the amount of Rvs by 20 molecules decreases scission efficiency to about 90% from 97% (supplemental material). This indicates that a particular coverage of the membrane tube is required for effective scaffolding by BAR domains. In support of this, in BAR strains, fewer numbers of Rvs are recruited, and scission efficiency is similarly reduced. At low concentrations of Rvs, some membrane tubes recruit the critical number of Rvs, in which case the membrane grows to near WT lengths. Over a certain amount of Rvs, adding more BAR domains does not increase the stability of the tube: in 4xd, the same amount of actin is recruited before scission as in the 2xd and 1xd strains.

If enough forces are generated at 60nm, why is scission efficiency decreased in *rvs167Δ* compared to WT? Forces from actin may be at a threshold at this time in the endocytic timeline. There could be enough to sever the membrane, but not to sever reliably. The Rvs scaffold then keeps the network growing to accumulate enough actin to reliably cause scission. Controlling membrane tube length could also be a way for the cell to control the amount of cargo packed into the vesicle.

4.5 Role of other scission-stage proteins

4.5.1 Inp52 is likely involved in uncoating vesicles after scission

Deletion of Synaptojanin-like Inp52 does not affect the invagination depths of Sla1. In spite of this, Sla1 patches persist for longer after scission in the *inp52Δ* than in WT cells, as does Rvs167 centroid, indicated by the arrows in Fig.3.7 A, D. Persistence in both suggests that rather than the scission time-point, post- scission disassembly of proteins from the vesicle is inhibited by *inp52Δ*, and that Inp52 plays a role in recycling endocytic proteins to the plasma membrane. The slower assembly of Rvs in *inp51Δ* and the decrease in scission efficiency of *inp52Δ* could indicate that there is a slight effect on Rvs recruitment, and that lipid hydrolysis could play a small role in scission.

4.6 Model for membrane scission

I propose that Rvs is recruited to sites by two distinct mechanisms. SH3 domains cluster Rvs at endocytic sites. This increases the efficiency with which the BAR domain senses membrane curvature. The BAR domain binds to endocytic sites by sensing tubular membranes. BAR domains interact with the entire membrane tube, but without forming a tight helical scaffold. BAR-membrane interactions prevent actin forces from causing membrane scission, and the invaginations continue to grow in length, as actin continues to polymerize and exert forces on the membrane. BAR recruitment to membrane tubes is restricted by the surface area of the tube: after a certain amount of Rvs, the excess interacts with endocytic sites via the SH3 domain. Adding over a certain amount of Rvs also does not increase the stabilization effect on the tube. As actin continues to polymerize, at a certain amount of actin, enough forces are generated to overcome the resistance to membrane scission provided by the BAR scaffold. The membrane ruptures, and vesicles are formed. Synaptojanins might help the recruitment of Rvs at endocytic sites: Inp51 and Inp52 have proline rich regions that could act as binding sites for SH3

domains. They are involved in vesicle uncoating post-scission, likely by phosphorylation regulation of endocytic proteins remaining on the vesicle.

4.7 Other potential scission mechanisms and open questions

Dmitrieff2015a clustering induces scission cooperation between lipid hydrolysis and actin forces?

why these curvatures? specificity from the SH3 domain? why does it come off regulation of activity? phosphorylation/ autoinhibition

5 | Materials and Methods

5.1 Materials

5.1.1 Yeast strains

STRAIN	GENOTYPE
MKY0100	MAT α , his3 Δ 200, leu2-3,112, ura3-52, lys2-801
MKY0102	MAT α , his3 Δ 200, leu2-3,112, ura3-52, lys2-801
	MAT α /MAT α , his3 Δ 200/his3 Δ 200, leu2-3,112/leu2-3,112, ura3-52/ura3-52,
MKY0105	lys2-801/lys2-801
MKY0122	MAT α , his3 Δ 200, leu2-3,112, ura3-52, lys2-801, ABP1-EGFP::HIS3MX6
MKY0123	MAT α , his3 Δ 200, leu2-3,112, ura3-52, lys2-801, ABP1-EGFP::HIS3MX6
MKY0216	MAT α his3 Δ 200, leu2-3,112 ura3-52, lys2-801 NUF2-EGFP::HIS3MX6
MKY0217	MAT α his3 Δ 200, leu2-3,112 ura3-52, lys2-801 NUF2-EGFP::HIS3MX6
MKY0224	MAT α , his3 Δ 200 leu2-3,112, ura3-52, lys2-801 NUF2-mCherry::KANMX4
MKY0225	MAT α his3 Δ 200, leu2-3,112 ura3-52, lys2-801 NUF2-mCherry::KANMX4
	MAT α , his3 Δ 200, leu2-3,112, ura3-52, lys2-801,SLA1-EGFP::HISMX, ABP1-
MKY0822	mCherry::kanMX
	MAT α , his3 Δ 200, leu2-3,112, ura3-52, SLA1-EGFP::HISMX, ABP1-
MKY0823	mCherry::kanMX
MKY0141	MAT α , his3 Δ 200, leu2-3,112, ura3-52, lys2-801, SLA1-EGFP::HIS3MX6
MKY2832	Mat a, his3 Δ 200, leu2-3,112, ura3-52, lys2-801, Rvs167-EGFP::HIS3MX6
	MAT α , his3 Δ 200, leu2-3,112, ura3-52, lys2-801, Abp1-mCherry::KANMX4,
MKY3131	Rvs167-EGFP::HISMX6
	MAT α , his3 Δ 200, leu2-3,112, ura3-52, lys2-801, Abp1-mCherry::KANMX4,
MKY3132	Rvs167-EGFP::HISMX6
	Mat a, his3 Δ 200, leu2-3,112, ura3-52, lys2-801, rvs167- Δ SH3-
MKY3154	EGFP::HIS3MX6
	MAT α , his3 Δ 200, leu2-3,112, ura3-52, lys2-801, rvs167- Δ SH3::natNT2, ABP1-
MKY3201	EGFP::HIS3MX6

	Mat a/α, his3Δ200/his3Δ200, leu2-3,112/leu2-3,112, ura3-52/ura3-52, lys2-
MKY3258	801/lys2-801,Vps1-EGFP::HIS3MX6/Vps1, Abp1-mCherry::KANMX/Abp1
MKY3260	Mat a, his3Δ200, leu2-3,112, ura3-52, lys2-801, Vps1-sfGFP::URA3
	MAT α , his3Δ200, leu2-3,112, ura3-52, lys2-801, sla2::natNT2, rvs167-ΔSH3-
MKY3280	EGFP::HIS3MX6, SLA1-mcherry::kanMX5
	MAT α , his3Δ200, leu2-3,112, ura3-52, lys2-801, sla2::natNT2, rvs167-ΔSH3-
MKY3281	EGFP::HIS3MX6, SLA1-mcherry::kanMX5
	MAT α , his3Δ200, leu2-3,112, ura3-52, lys2-801, sla2::natNT2, RVS167-
MKY3282	EGFP::HIS3MX6, ABP1-mcherry::kanMX5
	MAT α , his3Δ200, leu2-3,112, ura3-52, lys2-801, sla2::natNT2, RVS167-
MKY3283	EGFP::HIS3MX6, ABP1-mcherry::kanMX5
	MAT α , his3Δ200, leu2-3,112, ura3-52, lys2-801, sla2::natNT2, rvs167-ΔSH3-
MKY3284	EGFP::HIS3MX6, ABP1-mcherry::kanMX5
	MAT α , his3Δ200, leu2-3,112, ura3-52, lys2-801, sla2::natNT2, rvs167-ΔSH3-
MKY3285	EGFP::HIS3MX6, ABP1-mcherry::kanMX5
	MAT α , his3Δ200, leu2-3,112, ura3-52, lys2-801, rvs167-ΔSH3-
MKY3286	EGFP::HIS3MX6, ABP1-mCherry::KANMX4
MKY3287	MAT α , his3Δ200, leu2-3,112, ura3-52, lys2-801 rvs167-ΔSH3::natN2
MKY3288	MAT α , his3Δ200, leu2-3,112, ura3-52, lys2-801, rvs167-ΔSH3::natNT2
	MAT α , his3Δ200, leu2-3,112, ura3-52, lys2-801, rvs167-ΔSH3::natNT2, SLA1-
MKY3289	EGFP::HIS3MX6
	MAT α , his3Δ200, leu2-3,112, ura3-52, lys2-801, rvs167-ΔSH3::natNT2, SLA1-
MKY3290	EGFP::HIS3MX6
	MAT α , his3Δ200, leu2-3,112, ura3-52, lys2-801, rvs167-ΔSH3::natNT2, ABP1-
MKY3291	EGFP::HIS3MX6
	MAT α , his3Δ200, leu2-3,112, ura3-52, lys2-801, rvs167-ΔSH3::natNT2, SLA1-
MKY3292	EGFP::HIS3MX, ABP1-mcherry::kanMX4
	Mat α his3Δ200, leu2-3,112, ura3-52, lys2-801, SLA1-mCherry::KANMX4,
MKY3295	sla2::NAT, RVS167-EGFP::HIS3MX6
MKY3339	MAT α , his3Δ200, leu2-3,112, ura3-52, lys2-801 vps1::natNT2
	MAT α , his3Δ200, leu2-3,112, ura3-52, lys2-801, vps1::natNT2, RVS167-
MKY3341	EGFP::HIS3MX6
	MAT α , his3Δ200, leu2-3,112, ura3-52, lys2-801, vps1::natNT2, RVS167-
MKY3342	EGFP::HIS3MX6
	MAT α , his3Δ200, leu2-3,112, ura3-52, lys2-801, vps1::natNT2, RVS167-
MKY3343	EGFP::HIS3MX6 , ABP1-mCherry::kanMX4
	MAT α , his3Δ200, leu2-3,112, ura3-52, lys2-801, vps1::natNT2, RVS167-
MKY3344	EGFP::HIS3MX6 , ABP1-mCherry::kanMX4

	MAT α , his3 Δ 200, leu2-3,112, ura3-52, lys2-801, vps1 Δ ::natNT2, SLA1-
MKY3345	EGFP::HIS3MX6
	MAT α , his3 Δ 200, leu2-3,112, ura3-52, lys2-801, vps1 Δ ::natNT2, SLA1-
MKY3346	EGFP::HIS3MX6
	MAT α , his3 Δ 200, leu2-3,112, ura3-52, lys2-801, vps1 Δ ::natNT2, SLA1-
MKY3347	EGFP::HIS3MX6 , ABP1-mCherry::kanMX4
MKY3559	MAT α , his3 Δ 200, leu2-3,112, ura3-52, lys2-801, Inp51-EGFP::HIS3MX6
MKY3560	MAT α , his3 Δ 200, leu2-3,112, ura3-52, lys2-801, Inp52-EGFP::HIS3MX6
MKY3561	MAT α , his3 Δ 200, leu2-3,112, ura3-52, lys2-801, inp51 Δ ::URA
	MAT α , his3 Δ 200, leu2-3,112, ura3-52, lys2-801, inp51 Δ ::URA, Sla1-
MKY3562	EGFP::HIS3MX6, Abp1-mCherry::KANMX4
MKY3586	MAT α his3 Δ 200, leu2-3,112, ura3-52, lys2-801 inp52 Δ ::hphNT1
MKY3587	MAT α his3 Δ 200, leu2-3,112, ura3-52, lys2-801 inp52 Δ ::hphNT1
	MAT α , his3 Δ 200, leu2-3,112, ura3-52, lys2-801, Rvs167-EGFP::HISMX6,
MKY3620	inp51 Δ ::URA
	MAT α , his3 Δ 200, leu2-3,112, ura3-52, lys2-801, Rvs167-EGFP::HISMX6,
MKY3621	inp51 Δ ::URA
	MAT α , his3 Δ 200, leu2-3,112, ura3-52, lys2-801, Rvs167-EGFP::HISMX6,
MKY3622	inp51 Δ ::URA
	MAT α , his3 Δ 200, leu2-3,112, ura3-52, lys2-801, Inp52-EGFP::HISMX6, Abp1-
MKY3623	mCherry::KANMX4
	MAT α , his3 Δ 200, leu2-3,112, ura3-52, lys2-801, Inp52-EGFP::HISMX6 Abp1-
MKY3624	mCherry::KANMX4
MKY3702	MAT α his3 Δ 200, leu2-3,112, ura3-52, lys2-801 RVS161::URA::RVS161
	MAT α , his3 Δ 200, leu2-3,112, ura3-52, lys2-801, RVS161::URA::RVS161,
MKY3703	RVS167::HPH::RVS167
	MAT α , his3 Δ 200, leu2-3,112, ura3-52, lys2-801, RVS161::URA::RVS161,
MKY3704	RVS167::HPH::RVS167
	MAT α his3 Δ 200, leu2-3,112, ura3-52, lys2-801 RVS167::HPH::RVS167, SLA1-
MKY3705	EGFP::HISMX6
	MAT α his3 Δ 200, leu2-3,112, ura3-52, lys2-801 RVS161::URA::RVS161
MKY3706	RVS167::HPH::RVS167 SLA1-EGFP::HISMX6 ABP1-mCherry::KANMX4
MKY3707	MAT α his3 Δ 200, leu2-3,112, ura3-52, lys2-801 RVS167::HPH::RVS167
	MAT α his3 Δ 200, leu2-3,112, ura3-52, lys2-801, Rvs167-
MKY3708	EGFP::his3MX6::hphNT1::Rvs167-EGFP::his3MX6
	MAT α his3 Δ 200, leu2-3,112, ura3-52, lys2-801 RVS167-EGFP::HPH::RVS167-
MKY3709	EGFP Abp1-mCherry

	MATa his3Δ200, leu2-3,112, ura3-52, lys2-801, RVS161::URA::RVS161, SLA1-
MKY3711	EGFP::HISMX, ABP1-mCherry::kanMX MATa, his3Δ200, leu2-3,112, ura3-52, lys2-801, Rvs167-
MKY3712	EGFP::his3MX6::hphNT1::Rvs167-EGFP::his3MX6, RVS161::URA::RVS161
MKY3713	MAT α , his3Δ200, leu2-3,112, ura3-52, lys2-801, rvs167-ΔSH3::natN2 MAT α , his3Δ200, leu2-3,112, ura3-52, lys2-801, rvs167-ΔSH3- EGFP::his3MX6::hphNT1::rvs167-ΔSH3-EGFP::his3MX6, ABP1-
MKY3714	mCherry::kanMX MAT α , his3Δ200, leu2-3,112, ura3-52, lys2-801, rvs167-ΔSH3- EGFP::his3MX6::hphNT1::rvs167-ΔSH3-EGFP::his3MX6, ABP1-
MKY3728	mCherry::kanMX, RVS161::URA::RVS161 MATa his3Δ200, leu2-3,112, ura3-52, lys2-801, Rvs167-EGFP::HISMX6 Abp1-
MKY3803	mCherry::KANMX4 MAT α his3Δ200, leu2-3,112, ura3-52, lys2-801, inp52Δ::hphNT1, Abp1-
MKY3804	mCherry::kanMX4 MAT α his3Δ200, leu2-3,112, ura3-52, lys2-801, inp52Δ::hphNT1, Rvs167-
MKY3805	EGFP::HIS3MX6 MATa his3Δ200, leu2-3,112, ura3-52, lys2-801, inp52Δ::hphNT1, Rvs167-
MKY3806	EGFP::HIS3MX6 MAT α , his3Δ200, leu2-3,112, ura3-52, lys2-801, rvs167- ΔSH3::natNT2::hphNT1::rvs167-ΔSH3::natNT2, SLA1-EGFP::HISMX, ABP1-
MKY3826	mCherry::kanMX MAT α , his3Δ200, leu2-3,112, ura3-52, lys2-801, inp52Δ::hphNT1, SLA1-
MKY3827	EGFP::HISMX, ABP1-mCherry::kanMX MATa/ALPHA his3Δ200, leu2-3,112, ura3-52, lys2-801 RVS161::URA::RVS161/RVS161::URA::RVS161, Rvs167- EGFP::his3MX6::hphNT1::Rvs167-EGFP::his3MX6/Rvs167- EGFP::his3MX6::hphNT1::Rvs167-EGFP::his3MX6, ABP1-
MKY3945	mCHerry::KANMX4/Abp1 MATa/ALPHA, his3Δ200, leu2-3,112, ura3-52, lys2-801, Rvs167-
MKY3946	EGFP::HIS3MX6/Rvs167-EGFP::HIS3MX6, ABP1-mCHerry::KANMX4/Abp1 MATa/ α , his3-delta200, leu2-3,112, ura3-52, RVS167- EGFP::HIS3MX6/rvs167delta::cgLEU2, rvs161delta::cgLEU2/RVS161, ABP1-
MKY3947	RFP::HIS3MX6/ABP1
MKY3948	MATa, his3Δ200, leu2-3,112, ura3-52, lys2-801, Inp53-EGFP::HIS3MX6

5.1.2 Plasmids

Plasmid cassettes used for endogenous tagging and gene deletions/duplication.

Name	Purpose
pFA6a-EGFP-HIS4MX	EGFP tag
pFA6a-mCherry-KanMX4	mCherry tag
pFA6a-natNT2	deletion
pks133	deletion, duplication
pFA6a-KiUra	deletion

5.1.3 Buffers

PEG buffer

Lithium acetate	100 mM
Tris-HCl pH 8	10 mM
EDTA pH 8	1 mM
Polyethylene glycol	4 % w/v

SORB buffer

Lithium acetate	100 mM
Tris-HCl pH 8	10 mM
EDTA pH 8	1 mM
Sorbitol	1 M

S buffer

K2HPO4 pH 7.2	10 mM
EDTA	10 mM
β-mercaptoethanol	50 mM
Zymolyase	50 µg/mL

Lysis Buffer

Sodium dodecyl sulphate (SDS)	2.5 % w/v
Tris-HCl pH 7.5	25 mM
EDTA	25 mM

5.1.4 Media

Media was kindly prepared by the EMBL and University of Geneva media kitchens, and by Anne-Sophie Riviera. Plates containing media were made by adding 2% w/v bacto agar.

Yeast extract Peptone Dextrose (YPD)

BactoYeast Extract	1 % w/v
Bacto Peptone	2 % w/v
Glucose	2 % w/v

Synthetic Complete (SC)

DifcoTM Yeast nitrogen base w/o amino acids	0.67 % w/v
Glucose	2 % w/v
Amino acid stock (SC)	10 % v/v

Amino acid stock (SC) –dissolved in 100 mL

H2O

Adenine	0.5 g
Leucine	10 g
Alanine, Arginine, Asparagine, Aspartic acid, Cysteine, Glutamine, Glutamic acid, Glycine, Histidine, Inositol, Isoleucine, Lysine, Methionine, para-Aminobenzoic acid, Phenylalanine, Proline, Serine, Threonine, Tryptophan, Tyrosine, Uracil, Valine. For auxotrophic selection, one amino acid is left out	
	2 g each

Sporulation plates

Potassium acetate	1 % w/v
Bacto Agar	2 % w/v
Amino acid stock (sporulation plate)	0.25 % v/v

Amino acid stock (sporulation plate)

Uracil, Histidine, Methionine	0.2 g
Leucine, Lysine	0.3 g

Antibiotic selection plates

Hygromycin B (Hph) (InvivoGen)	300 mg/L
Geneticin disulphate salt (G418) (Sigma)	200 mg/L
Nourseothricin (clonNAT) (Werner BioAgents)	100 mg/L

5.1.5 Imaging

Live-cell tracking

Microscope	IX81	Olympus
Objective	PlanApo 100x/1.45 TIRFM	Olympus
Camera (molecule number quantification)	Orca -ER	Hamamatsu
Fluorescent lamp (molecule number quantification)	X-CITE 120 PC	EXFO
Laser source for GFP excitation	Sapphire 488-100	Coherent
Laser source for RFP excitation	Compass 315M (561 nm)	Coherent
Camera	ImagEM EMCCD	Hamamatsu
Microscope (TIRF)	IX83	Olympus
Camera (TIRF)	Image mX2 EMCCD	Hamamatsu
Objective (TIRF)		
Laser source (TIRF)	VS-LMS	Visitron

Electron microscopy

Microscope	Tecnai F30 300kV FEG	FEI
Camera	4k Eagle	FEI

5.2 Methods

5.2.1 Fluorescent tagging yeast with PCR cassette insertion

Tagging or deletion of endogenous genes was done by homologous integration of the product of a Polymerase Chain Reaction using appropriate primers and a plasmid containing a selection cassette and fluorescent tag, or only selection cassette for gene deletions. Primers were designed according to Janke et al, 2004. PCRs used the Velocity Polymerase for fluorescent tagging, and Q5 for gene deletions using the NAT cassette. All fluorescently tagged genes have a C-terminus tag and are expressed endogenously. Gene deletions and fluorescent tags are checked by PCR. Vps1del and gene duplications were confirmed by sequencing.

5.2.2 Live-cell imaging

Sample preparation for live imaging

40 μ L Concanavalin A (ConA) was incubated on a coverslip for 10 minutes. 40 μ L Yeast cells incubated overnight at 25C in imaging medium SC-TRP was added to the coverslip after removing the ConA, and incubated for another 10 minutes. Cells were then removed, adhered cells were washed 3x in SC-TRP, and 40 μ L SC-TRP was finally added to the coverslip to prevent cells from drying.

Sample preparation for live imaging in LatA and Sorbitol treated cells

Cells went through the same procedure as above till the last washing step. Instead of SC-TRP, 100x diluted LatA, or Sorbitol at a final concentration of 0.2M in SC-TRP was added to the adhered cells. For LatA experiments, cells were incubated in LatA for 10 minutes before imaging. For sorbitol treatments, cells were imaged within 5 minutes of adding sorbitol.

Epifluorescent imaging for centroid tracking

Live-cell imaging was performed as in Picco et al. All images were

obtained at room temperature using an Olympus IX81 microscope equipped with a 100 \times /NA 1.45 PlanApo objective , with an additional 1.6x magnification lens and an EMCCD camera. The GFP channel was imaged using a 470/22 nm band-pass excitation filter and a 520/35 nm band-pass emission filter. mCherry epifluorescence imaging was carried out using a 556/20 nm band-pass excitation filter and a 624/40 band-pass emission filter. GFP was excited using a 488 nm solid state laser and mCherry was excited using a 561 nm solid state laser. Hardware was controlled using Metamorph software. For single-channel images, 80-120ms was used as exposure time. All dual-channel images were acquired using 250ms exposure time. Simultaneous dual-color images were obtained using a dichroic mirror, with TetraSpeck beads used to correct for chromatic abberation.

Epifluorescent imaging for molecule number quantification

Images were acquired as in Picco et al. Z-stacks of cells containing the GFP-tagged protein of interest, incubated along with cells containing Nuf2-GFP, were acquired using 400ms exposure using a mercury vapour lamp, on a CCD camera. Z stacks were spaced at 200nm.

TIRF imaging

TIRF microscopy was performed under similar conditions on an Olympus IX83 microscope. GFP was excited using a 488 nm solid state laser and mCherry was excited using a 561 nm solid state laser. Lasers, and shutters were controlled by Visitron Systems VS-Laser Control. VisiView software controlled the image acquisition and hardware-software feedback. Images were processed using ImageJ, quantification was done on R.

5.2.2.1 Live-cell Image analysis

Images were processed for background noise using a rolling ball radius of 90 pixels. Particle detection, and tracking was performed for a particle size of 6 pixels, using scripts that combine background subtraction with Particle Tracker and Detector, that can be found on ImageJ (<http://imagej.nih.gov>). Further analysis for centroid averaging, alignments between dual-color images and single channel images, for alignment to the reference Abp1 were done using scripts written in

Matlab (Mathworks) and R (www.r-project.org), written originally by Andrea Picco, and modified by me. Details of analysis can be found at Picco et al. All movement and intensity plots from centroid tracking show the average centroid with 95% confidence interval. All molecule number quantifications report either the median or maximum number of molecules with standard error of mean. Maximum number is preferred over median in cases when the rate of change of fluorescent intensity of two populations being compared are not similar, and the lifetime of the protein populations being compared are not similar. The median in this case underreports the differences in protein accumulation.

5.2.2.2 Cytoplasmic background quantification for BAR versus WT Rvs167-GFP

On a maximum intensity projection of time-lapse images, the average pixel intensity within a circle of set radius in the cytoplasm was measured. This circle is manually arranged so that cortical patches were excluded, and mean intensity was acquired for about 10 cells of each cell type. A fixed area outside the cells was drawn, and mean intensity was calculated to establish "background intensity". This background intensity was then subtracted from the mean intensity to obtain a rough measure of cytoplasmic intensity. The same was done for endocytic spots. For WT strain, cytoplasmic signal after subtracting background is measured as 1951.611 +/- 299.56 (arbitary units, average +/- SEM), with spot intensity 5486 +/- 1304.6 (arbitary units, average +/- SEM). For BAR strain, cytoplasmic signal is 2058 +/- 322 (arbitary units, average +/- SEM), spots are 4477 +/- 1144.7 (arbitary units, average +/- SEM). The ratio of spot intensity for WT to BAR strain is 1.22, so the WT spots are 1.2x brighter than the BAR spots measured in this way. Cytoplasmic background of BAR is comparable to that of the WT: the ratio of WT to BAR cytoplasmic signal obtained in this way is 0.94. Although this is not a stringent quantification of cytoplasmic intensity, with some caveats: the cells were not incubated in the same field of view, cellular autofluorescence is assumed to be equal for the two cell types, I take this measurement to indicate that the cytoplasmic content of BAR and WT Rvs167-GFP is not significantly different.

5.2.2.3 CLEM

Samples were prepared for CLEM as described in Wanda et al. Briefly, cells expressing Rvs167-GFP and Abp1-mCherry, and BAR-GFP and Abp1-mCherry cells were grown overnight in YPD, at 24C. They were then diluted to an OD₆₀₀ of 0.2, and grown to OD₆₀₀ between 0.8 and 1.2. These cells were then concentrated to a filter paper using a vacuum pump, and high-pressure frozen. Samples were freeze substituted in Lowycryl HM20 using the Kukulski freeze substitution protocol using an automated robot. Samples in resin were sliced to 300nm sections using a diamond knife, and loaded to carbon-coated copper grids. TetraSpec beads were incubated on the slices and these slices were imaged using epifluorescence microscopy in GFP and RFP channels for GFP and m-Cherry, and Cyan channel for separating the signal from the Tetraspec beads, that would later be used as fiducials to correlate these fluorescent images with electron tomograms. Gold fiducials were incubated on the grids, and lead citrate was added to stain the membrane. Low magnification tilts were acquired at 3 degree increments. High magnification tilts were performed at 1 degree increments from -60 to 60 degrees. Tomograms were reconstructed using IMOD. Invagination lengths were measured at the longest axis of the invagination, using IMOD.

Bibliography

- coordinates protein-protein interactions essential for endocytosis’, *Rockefeller University Press*, 141(1), pp. 71–84. doi: 10.1089/bbamcr.2010.08.013.
- Wong, M. H., Meng, L., Rajmohan, R., Yu, S. and Thanabalu, G. (2008) ‘The yeast amphiphysin Rvs161p is critical for actin patch polarization but is not essential for growth’, *Biochimica et biophysica acta*, 1803(12), pp. 1333–1341. doi: 10.1016/j.bbamcr.2010.08.013.
- Yidi Sun, A. C. M. (2006) ‘Endocytic internalization in budding yeast requires Arf1 GTPase, clathrin-mediated nucleation and myosin motor activity.’, *Developmental cell*, 11(5), pp. 631–642. doi: 10.1016/j.devcel.2006.05.008.
- Youn, J.-Y., Friesen, H., Kishimoto, T., Henne, W. M., Kurat, S., Kohlwein, S. D., McMahon, H. T. and Andrews, B. J. (2010) ‘Yeast Amphiphysins Rvs161 and Rvs167 during Endocytosis’, *Molecular Biology of the Cell*, 21(14), pp. 3054–3069. doi: 10.1091/mbc.E10-03-0181.
- Yu, X. (2004) ‘The yeast dynamin-related GTPase Vps1p functions at the plasma membrane by interacting with the cytoskeleton via interaction with Sla1p’, *Journal of Cell Science*, 117(18), pp. 4751–4760. doi: 10.1242/jcs.01239.
- Zhang, P. and Hinshaw, J. E. (2001) ‘Three-dimensional reconstruction of the yeast vesicle fusion complex in its inactive state’, *Nature Cell Biology*. Nature Publishing Group, 3(10), pp. 915–922. doi: 10.1038/35106070.
- Zhao, W.-D., Hamid, E., Shin, W., Wen, P. J., Krystofiak, E. S., Li, Y., Wang, Y., Liu, Y., Zhou, Y., Guo, Y., Wang, Y., Li, B. and Wu, L.-G. (2016) ‘Hemi-fused structure mediates and stabilizes the yeast vesicle fusion complex’, *Nature*. NIH Public Access, 534(7608), pp. 548–552. doi: 10.1038/nature18600.